

Investigating the effects of tropomyosin mutations on its flexibility and interactions with filamentous actin using molecular dynamics simulation

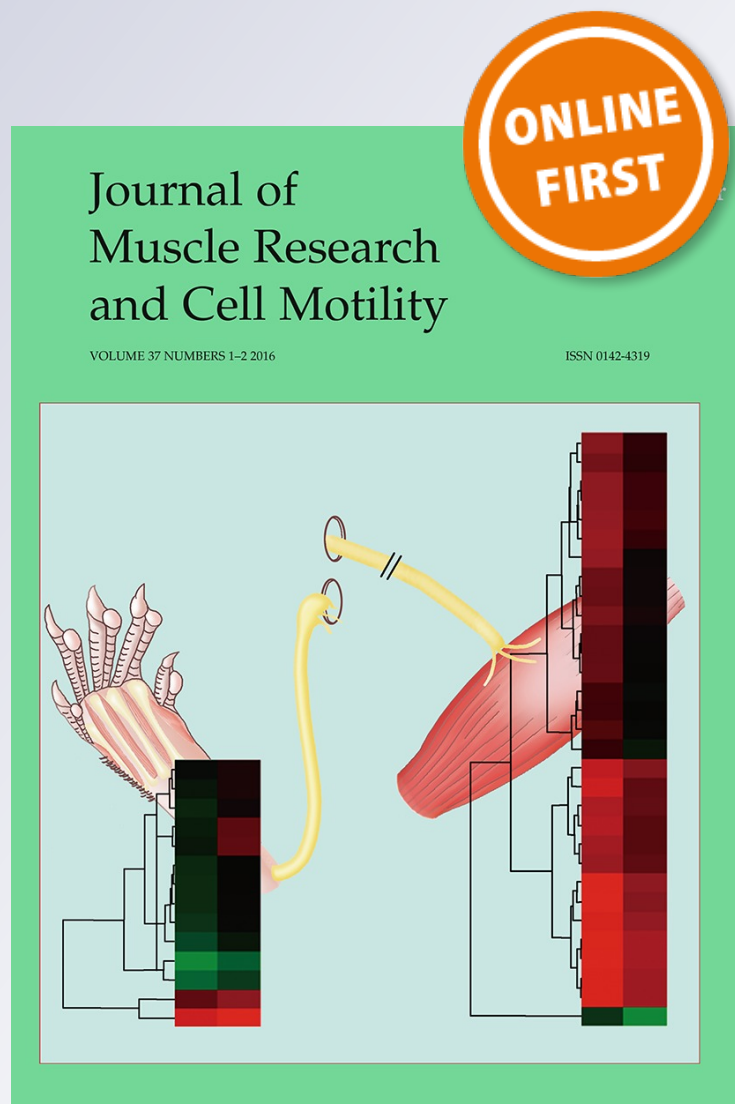
Wenjun Zheng, Sarah E. Hitchcock-DeGregori & Bipasha Barua

Journal of Muscle Research and Cell Motility

ISSN 0142-4319

J Muscle Res Cell Motil

DOI 10.1007/s10974-016-9447-3



Your article is protected by copyright and all rights are held exclusively by Springer International Publishing Switzerland. This e-offprint is for personal use only and shall not be self-archived in electronic repositories. If you wish to self-archive your article, please use the accepted manuscript version for posting on your own website. You may further deposit the accepted manuscript version in any repository, provided it is only made publicly available 12 months after official publication or later and provided acknowledgement is given to the original source of publication and a link is inserted to the published article on Springer's website. The link must be accompanied by the following text: "The final publication is available at link.springer.com".

Investigating the effects of tropomyosin mutations on its flexibility and interactions with filamentous actin using molecular dynamics simulation

Wenjun Zheng¹ · Sarah E. Hitchcock-DeGregori² · Bipasha Barua²

Received: 23 January 2016 / Accepted: 24 June 2016
© Springer International Publishing Switzerland 2016

Abstract Tropomyosin (Tpm) is a two-chained α -helical coiled-coil protein that binds to filamentous actin (F-actin), and regulates its interactions with myosin by occupying three average positions on F-actin (blocked, closed, and open). Mutations in the Tpm are linked to heart diseases including hypertrophic cardiomyopathy (HCM) and dilated cardiomyopathy (DCM). To elucidate the molecular mechanisms of Tpm mutations (including DCM mutation E54K, HCM mutations E62Q, A63V, K70T, V95A, D175N, E180G, L185R, E192K, and a designed synthetic mutation D137L) in terms of their effects on Tpm flexibility and its interactions with F-actin, we conducted extensive molecular dynamics simulations for the wild-type and mutant Tpm in complex with F-actin (total simulation time 160 ns per mutant). The mutants exhibited distinct changes (i.e., increase or decrease) in the overall and local flexibility of the Tpm coiled-coil, with each mutation causing both local and long-range modifications of the Tpm flexibility. In addition, our binding calculations revealed weakened Tpm–F-actin interactions (except for L185R, D137L and A63V) involving five periods of Tpm, which correlate with elevated fluctuation of Tpm relative to the blocked position on F-actin that may lead to easier

activation and increased Ca^{2+} -sensitivity. We also simulated the $\alpha\beta/\beta\alpha$ -Tpm heterodimer in comparison with the $\alpha\alpha$ -Tpm homodimer, which revealed greater flexibility and weaker actin binding in the heterodimer. Our findings are consistent with a complex mechanism underlying how different Tpm mutations perturb the Tpm function in distinct ways (e.g., by affecting specific sites of Tpm), which bear no simple links to the disease phenotypes (e.g., HCM vs. DCM).

Keywords Binding energy · Cardiomyopathy · F-actin · Flexibility · Molecular dynamics · Mutation · Persistent length · Tropomyosin

Introduction

Tropomyosin (Tpm) (Geeves et al. 2015) is a prototype α -helical coiled-coil consisting of a sequence of heptad amino acid repeats denoted as $(abcdefg)_n$, which is stabilized by hydrophobic core residues at *a* and *d* positions and oppositely charged residues at *e* and *g* positions. The canonical core residues of Tpm are subject to irregular interruptions by destabilizing residues (Kwok and Hodges 2004), including six clusters of alanines [named “Ala clusters” (Brown et al. 2001; Kwok and Hodges 2004; McLachlan et al. 1975)], two acidic residues (D137 and E218) and other polar residues (Minakata et al. 2008). Tpm regulates the cooperative binding of actin-binding proteins (e.g., myosin) with filamentous actin (F-actin) in muscle and non-muscle cells (Gunning 2008), and the assembly and dynamics of F-actin (Khaitlina 2015). There are two main Tpm isoforms (α and β , or Tpm 1.1 and Tpm 2.2 in the new nomenclature, see (Geeves et al. 2015) in striated muscles, which form $\alpha\alpha$ homodimers or $\alpha\beta$ heterodimers.

Electronic supplementary material The online version of this article (doi:10.1007/s10974-016-9447-3) contains supplementary material, which is available to authorized users.

✉ Wenjun Zheng
wjzheng@buffalo.edu

¹ Department of Physics, University at Buffalo, 239 Fronczak Hall, Buffalo, NY 14260, USA

² Department of Pathology and Laboratory Medicine, Robert Wood Johnson Medical School, Rutgers University, Piscataway, NJ 08854, USA

Extensive structure–function analyses have been conducted for Tpm mutations that are linked to hypertrophic cardiomyopathy (HCM) and dilated cardiomyopathy (DCM) (Marston 2011), and skeletal muscle myopathy (Marston et al. 2013; Marttila et al. 2012; Yuen et al. 2015). As revealed by electron microscopy (EM) studies of Tpm-decorated F-actin, Tpm adopts three average azimuthal positions (i.e. blocked, closed, and open position) on the surface of F-actin that either block or unblock/activate the binding of myosin (Behrmann et al. 2012; Craig and Lehman 2001; Lehman and Craig 2008; Pirani et al. 2005, 2006; Poole et al. 2006; Sousa et al. 2013; Vibert et al. 1997; von der Ecken et al. 2015). Recent breakthroughs in cryo-EM have enabled improved visualization of Tpm on F-actin at sub-nanometer resolutions (Behrmann et al. 2012; Sousa et al. 2013; von der Ecken et al. 2015). Nevertheless, because of the use of low temperature, helical averaging in the reconstructions, and limits in the resolution of Tpm (>6 Å), although the coiled coil is well-resolved, the variations of the Tpm–actin interfaces along the length of Tpm, configuration of the side chains of Tpm that bind actin subunits, and the molecular ends of Tpm are lost. Although various models were proposed (Li et al. 2011; Lorenz et al. 1995; Pirani et al. 2006), no near-atomic-resolution structure has been solved experimentally to date for full-length Tpm in complex with actin. The binding of Tpm with F-actin involves seven quasi-equivalent regions [i.e., periods P1–P7, see Barua et al. (2011, 2013) for ranges of residue numbers] which participate in actin binding with different contributions (Hitchcock-DeGregori and Singh 2010; Hitchcock-DeGregori et al. 2001). To fulfill its regulatory function, Tpm must adopt a superhelical conformation to wrap around the F-actin helix, which can be achieved by either pre-shaping Tpm to match F-actin's helical shape (Holmes and Lehman 2008), or via flexible conformational sampling (Hitchcock-DeGregori and Singh 2010). A major source of flexibility is the non-canonical destabilizing regions including six Ala clusters (Brown et al. 2001; Kwok and Hodges 2004; McLachlan et al. 1975), where local axial staggering between two Tpm chains could induce local bending of Tpm backbones (Brown et al. 2001; Brown et al. 2005). Additionally, side-chain flexibility may result from poor packing in the destabilizing regions of Tpm (Singh and Hitchcock-DeGregori 2006). The elastic properties of Tpm coiled-coil were characterized in a computational study (Lakkaraju and Hwang 2009). By treating overlapping Tpm as a continuous flexible chain, Mijailovich et al. (2012) modeled the regulation of striated muscle contraction involving cooperative interactions between actin filaments, myosin-S1, Tpm, troponin, and calcium. Note that the widely used term of “protein flexibility” manifests in different forms including local atomic

fluctuations, global shape deformation or unfolding. In this study, we will focus on the fast atomic fluctuations that are accessible to molecular simulation (see below).

Molecular dynamics (MD) is the method of choice for simulating protein dynamics with atomic detail in the presence of water and ions under physiological conditions (Karplus and McCammon 2002). Previous MD simulation studies have provided rich structural and dynamic information for the shape and flexibility of Tpm (Lehman et al. 2014; Li et al. 2010a, b, c, 2011, 2014; Zheng et al. 2013), for the effects of Tpm mutations (Li et al. 2012; Moore et al. 2011), and for actin dynamics (Zheng et al. 2007). In complement with the MD approach, an energy landscape method was recently used to probe how disease mutations perturb the interactions between Tpm and F-actin as rigid bodies (Marston et al. 2013; Orzechowski et al. 2014).

In the past, for a large biomolecular system like the Tpm–F-actin complex with explicit solvent, MD simulation has been highly expensive, demanding the use of a massively parallelized or special-purpose supercomputer. Thanks to recent developments in computing hardware and software [particularly the use of graphics processing units to accelerate MD simulation (Stone et al. 2010)], one can now routinely run MD simulation of a large system (with several hundred thousand atoms) at a speed of a few ns/day on a single computer node. This allows effective sampling of the conformational space for an equilibrium state of a protein complex by simultaneously running multiple MD trajectories (Caves et al. 1998).

Previous MD studies by Lehman and coworkers (Li et al. 2010a, b, c, 2011) found that the average Tpm conformation is pre-shaped for binding F-actin, and the Tpm flexibility is highly delocalized rather than being localized in the destabilizing regions of Tpm (Li et al. 2010c). In a recent study (Zheng et al. 2013), we conducted extensive MD simulations for both the Tpm alone and the Tpm–F-actin complex. In contrast to Lehman et al. (Li et al. 2010c), we introduced and analyzed new flexibility parameters that specifically probe the local packing of the Tpm coiled-coil, and found a clear correlation between the regions with high local flexibility and the known destabilizing regions of Tpm (including six Ala clusters). Such robust correlation persists in the absence and presence of F-actin. In addition, we performed Tpm–F-actin binding calculations based on the MD simulations, which allowed us to identify key residues of Tpm involved in its dynamic interactions with F-actin [for details, see Table S4 and Figure S9 in (Zheng et al. 2013)]. The above study has established a computational framework for investigating the Tpm flexibility and Tpm–F-actin binding with amino-acid level of detail.

In the present study, we have utilized the MD simulation/analysis established in our previous study (Zheng et al.

2013) to investigate the effects of Tpm mutations and isoform differences on its flexibility and binding with F-actin, which underlie the molecular mechanisms of various disease mutations of Tpm. This extensive simulation study encompasses ten Tpm mutants (E54K, E62Q, A63V, K70T, V95A, D137L, D175N, E180G, L185R, and E192K) and two Tpm heterodimers ($\alpha\beta$ and $\beta\alpha$, with chain B or A of the $\alpha\alpha$ -Tpm replaced by β -Tpm, see Fig. 1a) with 160 ns per system in simulation time. This simulation offers detailed insights as to how these mutations perturb the global and local flexibility of Tpm and its interactions with F-actin (e.g., affecting specific regions of Tpm), leading to functional alterations as observed experimentally and clinically. Such molecular details will guide future study of disease mechanisms and aid development of therapeutic agents. Our simulation-based approach is complementary to the experimental structural-biology study of Tpm by providing key details of dynamics and energetics absent in the static models of Tpm obtained previously.

Methods

System setup and MD simulation

A model of the full-length $\alpha\alpha$ -Tpm dimer in complex with a 15-actin filament was constructed by the Lehman lab (Li et al. 2011) based on a computational search optimizing the electrostatic interactions for multiple azimuthal locations, z-positions, and pseudo-rotations of Tpm on F-actin. Starting from this initial model, we introduced point mutations in Tpm using the VMD program (Humphrey et al. 1996), and used the Swiss modeler server (<http://swissmodel.expasy.org/>) to model β -Tpm in the $\alpha\beta$ and $\beta\alpha$ -Tpm heterodimer. Following (Zheng et al. 2013), we setup 13 systems of the solvated and ionized Tpm–F-actin complex for the WT Tpm, 10 Tpm mutants, and 2 Tpm heterodimers ($\alpha\beta$ and $\beta\alpha$). The hydrogen atoms were added with VMD. The proteins were immersed into a rectangular box of water molecules extending 8–10 Å from the proteins in each direction by using VMD. To ensure a physiological ionic concentration of 0.15 M and zero net charge, Na^+ and Cl^- ions were added to the systems by VMD. The entire system contains $\sim 658,000$ atoms.

The systems were refined with two rounds of energy minimization using the steepest descent method: first, a 5000-step energy minimization was carried out with harmonic constraints (force constant = 10 kcal/mol/Å²) applied to all protein backbone heavy atoms, then a 5000-step energy minimization was conducted with harmonic constraints (force constant = 0.01 kcal/mol/Å²)

applied to C α atoms only. The systems were then heated to 300 K over 300 ps by MD with harmonic constraints (force constant = 0.01 kcal/mol/Å²) applied to C α atoms only, after which the systems were equilibrated for 500 ps with MD in the NVT ensemble with the same constraints as in heating. Finally, the systems were subject to a 20-ns production MD run in the NPT ensemble with harmonic constraints (force constant = 0.01 kcal/mol/Å²) applied to the C α atoms of F-actin only. These weak restraints maintain the global stability of F-actin while allowing local fluctuations of the backbones (~ 2 Å in RMSD) and full flexibility of the sidechains. The Nosé–Hoover method (Martyna et al. 1999) was used with temperature $T = 300$ K and pressure $P = 1$ atm. The periodic boundary conditions were applied to the systems. A 10-Å switching distance and a 12-Å cutoff distance were used for non-bonded interactions. The particle mesh Ewald (PME) method (Deserno and Holm 1998) was used to calculate long-range electrostatic interactions. The SHAKE algorithm (Hoover 1985) was used to constrain the bond lengths of hydrogen-containing bonds, which allows a time step of 2 fs for MD simulations. The atomic coordinates of the systems were saved for later analysis every 20 ps during MD simulations. The energy minimization and MD simulation were carried out with the NAMD program version 2.9b2 (Phillips et al. 2005) using the CHARMM27 force field (MacKerell et al. 1998) and TIP3P water model (Mackerell et al. 2004). See Zheng et al. (2013) for further analysis of the convergence of MD simulations.

Local flexibility analysis of the Tpm coiled-coil on F-actin

For core residues of a Tpm dimer comprised of two α -helical chains (named A and B), we calculated the following three flexibility parameters as defined in (Zheng et al. 2013) (see Fig. 1b): D_{ad} measures the average distance between the d residue of chain A and the a' and a'' residues of chain B at the coiled-coil interface. D_{AS} measures the axial displacement of the d residue of chain A along the a' – a'' direction, where a large $|D_{AS}|$ indicates a large axial staggering (AS) of this residue relative to chain B (Brown et al. 2001). D_{\perp} measures the perpendicular distance between the d residue of chain A and the line a' – a'' , which is related to the local diameter of the Tpm coiled-coil (Brown 2010). The above parameters were also defined for each a residue of chain A packed between two adjacent d residues of chain B (Zheng et al. 2013). D_{AS} and D_{\perp} quantify the axial and lateral motion between the two Tpm chains, respectively (see Fig. 1b). D_{ad} is affected by both of these motions.

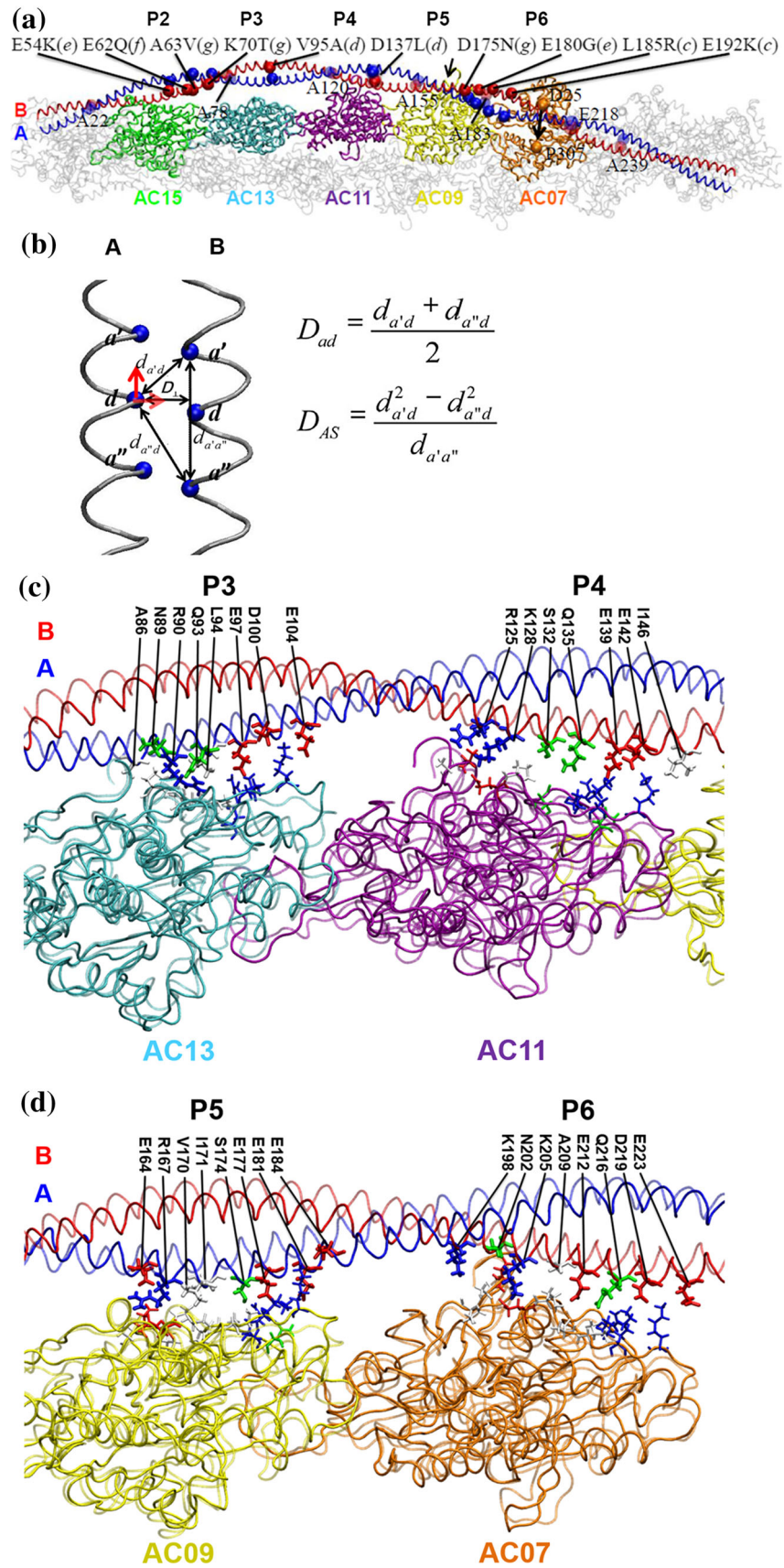


Fig. 1 a Structural view of the full-length Tpm dimer in complex with F-actin at the blocked position: five actin subunits (AC07–AC15, colored orange, yellow, purple, cyan, and green) interact with periods P2–P6 [see Barua et al. (2013) and Barua et al. (2011) for ranges of residue numbers] of Tpm dimer comprised of chain A (blue) and B (red). In the $\alpha\beta$ ($\beta\alpha$) heterodimer, chain A (B) is α -Tpm and chain B (A) is β -Tpm. Residues involved in ten Tpm mutations [E54K(e), E62Q(f), A63V(g), K70T(g), V95A(d), D137L(d), D175N(g), E180G(e), L185R(c), and E192K(c), where the heptad position is in parenthesis] are shown as opaque spheres. Core residues of the six Ala clusters ALA1–ALA6 (A22, A78, A120, A155, A183, and A239) and two destabilizing residues (D137 and E218) are shown as transparent spheres. The two marker residues (D25 and P307 for the blocked and open position) on F-actin are shown on one actin subunit (AC07). The movement of Tpm from the blocked to the open position is marked by an arrow. **b** The hydrophobic interface between chains A and B of the Tpm coiled coil is shown. Three core residues in each chain (at the a' , d , and a'' positions) are shown as spheres, and the distances between these residues and the perpendicular distance D_{\perp} are shown by double-headed arrows. The two orthogonal motions (i.e., axial and lateral motion) of the d residue in chain A relative to chain B are highlighted by two bold arrows. Residue contacts between c period P3 and P4, d period P5 and P6 of Tpm and two adjacent actin subunits from a representative MD snapshot. Contacting residues are colored as follows: acidic (red), basic (blue), polar (green), non-polar (light gray). For comparison, the MD snapshot is shown as opaque while the initial model is shown as transparent. Note that some hydrophobic residues of Tpm (e.g., V170 and I171) form close contacts with actin residues. (Color figure online)

Global flexibility analysis of Tpm on F-actin

To assess the global flexibility of Tpm based on the last 10 ns of MD simulation, we calculated the root mean squared fluctuation (RMSF) after superimposing C α atomic coordinates of 500 MD snapshots along Tpm (or F-actin) following (Zheng et al. 2013), then we calculated the following root mean squared average of RMSF over all Tpm residues: $\langle \text{RMSF} \rangle_{\text{Tpm or F-actin}} = \sqrt{\frac{1}{N} \sum_{n=1}^N \text{RMSF}_n^2}$, where $N = 568$ is the number of residues in the Tpm coiled-coil (284 residues per chain), and the subscript indicates superposition along Tpm or F-actin.

The Tpm–actin binding calculation

We used a continuum solvent model to estimate the binding free energy, which has been extensively applied by us (Li and Zheng 2011, 2012) and others [see refs in Eriksson and Roux (2002)] as a useful and inexpensive way to calculate and compare the binding free energies of various protein complexes and their mutants. Following (Zheng et al. 2013), based on the last 10 ns of MD simulation, we calculated the Tpm–actin binding free energy ΔG for each of the five actin subunits interacting with periods P2–P6 of Tpm (periods P1 and P7 were excluded because they are in the overlap regions which are not properly modeled here).

Here ΔG is expressed as $\Delta G = \Delta G_{\text{np}} + \Delta G_{\text{elec}}$, where the nonpolar contribution $\Delta G_{\text{np}} = \alpha E_{\text{vdW}}$ is a fraction of the van der Waals (vdW) interaction energy E_{vdW} between Tpm and actin in the Tpm–actin complex, and the electrostatic contribution $\Delta G_{\text{elec}} = \beta \Delta E_{\text{elec}}$ is a fraction of the change in electrostatic energy ΔE_{elec} from the unbound Tpm and actin to the Tpm–actin complex. Here we assume the vdW interaction energy is zero for the unbound Tpm. $\alpha = 0.08$ and $\beta = 0.12$ were obtained from the fitting of actin–Tpm binding data for five Tpm mutants (see Table S4). The finding of $\alpha < \beta$ suggests greater importance of the electrostatic energy than the vdW energy. However, the vdW energy is numerically larger (see Table 3), so even after weighting by a smaller α , the vdW contribution remains as significant as the electrostatic contribution to ΔG . E_{elec} was calculated using the Poisson–Boltzmann (PB) method (Gilson and Honig 1988; Im et al. 1998). For the PB calculation (Gilson and Honig 1988; Im et al. 1998), a dielectric constant $\epsilon_i = 4$ was used for the protein interior (Gilson and Honig 1986; Olson and Reinke 2000; Sharp and Honig 1990a, b), and $\epsilon_e = 80$ was used for the exterior aqueous environment. A probe radius of 1.4 Å (the approximate radius of a water molecule) was used to define the molecular surface corresponding to the dielectric boundary. The salt concentration was set to 0.12 M which approximately corresponds to a typical buffer condition of 100 mM KCl. All the PB calculations were performed using the PBEQ module (Im et al. 1998; Nina et al. 1997; Roux 1997) of CHARMM program (Brooks et al. 1983). The atomic Born radii used here were previously calibrated in (Nina et al. 1997). The calculated ΔG does not include the entropic contribution, so cannot be directly compared with experimentally measured binding affinity.

Results and discussion

Because of the lack of high-resolution structural information for full-length Tpm in complex with actin, we ran MD simulations starting from a computational model (Li et al. 2011) to investigate the dynamics and energetics of the Tpm–F-actin interaction and how they are affected by Tpm mutations and isoform differences. This model was validated by docking atomic structures of F-actin and Tpm into EM maps of F-actin–Tpm complex (Li et al. 2011), and the actin-binding sites predicted by this model were tested and supported by mutational studies (Barua et al. 2011, 2013). The main reason for choosing this model is because it captures a full-length Tpm near the low-Ca²⁺ blocked (B) state, whose destabilization may account for the high Ca²⁺-sensitivity observed in many HCM mutants (Redwood and Robinson 2013). In contrast, the recent higher-

resolution structures constructed from cryo-EM only captured the middle part of Tpm near the closed or open position on F-actin (Behrmann et al. 2012; Sousa et al. 2013; von der Ecken et al. 2015). So we did not choose these cryo-EM structures for our MD simulations. The molecular details gained by our simulation will help to understand and guide functional and clinical studies of Tpm mutants. We will first discuss the various analyses with examples that highlight our findings. Then we will give a detailed discussion of the effects of individual mutations in a separate section.

MD simulations of Tpm bound with F-actin

To fully explore the dynamics of a Tpm dimer interacting with F-actin in the presence of water and ions, we constructed 13 systems for the WT $\alpha\alpha$ -Tpm dimer, 10 α Tpm mutants [E54K(*e*), E62Q(*f*), A63V(*g*), K70T(*g*), V95A(*d*), D137L(*d*), D175N(*g*), E180G(*e*), L185R(*c*), and E192K(*c*), where the heptad position is in parenthesis], and $\alpha\beta$ and $\beta\alpha$ -Tpm dimer in complex with a 15-subunit F-actin (see “Methods” section and Fig. 1a). Then we completed eight 20-ns-long MD simulations of each system (total simulation time is 160 ns per system). To our knowledge, this is to date the most extensive MD study of the Tpm–F-actin complex and Tpm mutants, enabling us to investigate the impact of Tpm mutations and isoform differences on the flexibility and actin binding of Tpm.

To assess the stability of our simulations, we analyzed the root mean squared deviation (RMSD) relative to the initial model of Tpm for each MD trajectory. Despite large fluctuations, the RMSD stabilizes within 10 ns (e.g., for the WT, $\text{RMSD} = 3.8 \pm 0.9 \text{ \AA}$ in the last 10 ns of simulation, see Table 1). Therefore, following (Zheng et al. 2013), we combined the conformations sampled by the last 10 ns of 8 MD trajectories to generate a structural ensemble for

analysis of Tpm flexibility and Tpm–F-actin binding (see below). Because of the flexibility of Tpm and F-actin, Tpm moves closer to F-actin by $\leq 2 \text{ \AA}$ (relative to the other structural models, see Table S2 and S3), allowing more atomic contacts to form between them involving both charged and non-charged residues (see Fig. 1c, d). Therefore, the notion that the Tpm is too far away from F-actin (with minimal distance of 7–8 \AA , see Table S2) to allow non-polar interactions (Lorenz et al. 1995) may need to be revised for Tpm featuring local instability and flexibility (Hitchcock-DeGregori and Singh 2010). During simulation, the Tpm mostly fluctuates near the blocked position captured by the initial model, without undergoing any unfolding or large shift to the closed/open positions.

Global flexibility analysis of Tpm on F-actin

To explore the overall flexibility of Tpm in terms of atomic fluctuations near the average structure, we calculated the root mean squared fluctuation (RMSF) at each residue position of Tpm (denoted as $\text{RMSF}_{\text{TpmorF-actin}}$), after superimposing the $C\alpha$ coordinates of Tpm, or superimposing the $C\alpha$ coordinates of F-actin (see “Methods” section). The former (RMSF_{Tpm}) assesses the internal flexibility of Tpm, and the latter ($\text{RMSF}_{\text{F-actin}}$) assesses both internal flexibility and the mobility of Tpm relative to F-actin. Then we computed the average RMSF over all Tpm residues (denoted as $\langle \text{RMSF} \rangle_{\text{TpmorF-actin}}$, see “Methods” section) to assess the overall flexibility of Tpm. Compared with the WT (with $\langle \text{RMSF} \rangle_{\text{Tpm}} = 2.98 \text{ \AA}$), some Tpm mutants (e.g., E54K, V95A, E180G, and L185R) exhibit lower overall flexibility (with $2.63 \text{ \AA} \leq \langle \text{RMSF} \rangle_{\text{Tpm}} \leq 2.78 \text{ \AA}$, see Table 1), while others (e.g., E62Q, K70T, and D175N) show higher flexibility (with $3.33 \text{ \AA} \leq \langle \text{RMSF} \rangle_{\text{Tpm}} \leq 3.39 \text{ \AA}$, see Table 1).

Table 1 Summary of flexibility analysis based on MD simulations

System	Persistent length (\AA)	RMSD (\AA)	$\langle \text{RMSF} \rangle_{\text{Tpm}}$ (\AA)	$\langle \text{RMSF} \rangle_{\text{F-actin}}$ (\AA)
WT	877	3.8 ± 0.9	2.98	3.78
E54K	1172	3.4 ± 0.6	2.65	3.49
E62Q	644	4.4 ± 1.3	3.37	4.66
A63V	785	3.8 ± 0.6	3.09	4.12
K70T	1163	3.9 ± 0.9	3.33	4.45
V95A	1110	3.5 ± 0.7	2.78	3.64
D137L	1122	3.5 ± 0.8	2.92	3.90
D175N	865	4.1 ± 0.9	3.39	4.49
E180G	1115	3.4 ± 0.5	2.63	3.61
L185R	837	3.4 ± 0.6	2.70	3.53
E192K	1330	3.5 ± 0.5	2.86	3.67
$\alpha\beta$	977	3.8 ± 0.9	3.17	4.19
$\beta\alpha$	575	4.3 ± 1.0	3.21	3.86

Interestingly, $\langle \text{RMSF} \rangle_{\text{Tpm}}$ seems to correlate well with RMSD (with Pearson correlation = 0.90), indicating that Tpm mutants with higher overall flexibility deviate further from the initial Tpm coiled-coil structure (Li et al. 2011). $\langle \text{RMSF} \rangle_{\text{Tpm}}$ and $\langle \text{RMSF} \rangle_{\text{F-actin}}$ also correlate well (with Pearson correlation = 0.93), suggesting that Tpm mutants with higher internal flexibility tend to be more mobile on F-actin.

To complement the RMSF analysis and compare with other studies of Tpm flexibility (Li et al. 2010a, b, c, 2012; Loong et al. 2012a, b; Sousa et al. 2010), we have calculated the apparent persistent length (PL) with the commonly used tangent correlation method (also used in previous studies, see (Li et al. 2010b; Loong et al. 2012b)) for the WT and Tpm mutants (see Table 1). For the WT Tpm, we obtained a PL of 877 Å which is a little less than the value obtained for actin-free Tpm [~ 1000 Å, see Li et al. (2010b) and Sousa et al. (2010)], suggesting the Tpm is more curved upon binding to F-actin. For both WT and Tpm mutants, we found moderate correlation between PL and $\langle \text{RMSF} \rangle_{\text{Tpm}}$ or $\langle \text{RMSF} \rangle_{\text{F-actin}}$ (with Pearson correlation = -0.5), which is consistent with the idea that the PL not only depends on flexibility but also on the end-to-end curvedness of Tpm (Li et al. 2010b). For example, the K70T mutant is more flexible than the WT (with higher RMSF) but its PL is also greater than the WT due to smaller end-to-end curvedness (see Table 1). Given the heptad repeats in Tpm, one would expect a mutation at an *a* or *d* position (or changing a charged residue at an *e* or *g* position) will have a greater effect on the flexibility (stability) than those mutations at the *b*, *c*, or *f* positions. However, we did not observe significant correlation between RMSF or PL and the heptad positions of these mutations.

Local flexibility analysis of the Tpm coiled-coil on F-actin

Following (Zheng et al. 2013), to explore various aspects of local flexibility in the Tpm coiled coil, we calculated the following three parameters at each *a/d* position of Tpm (see “Methods” section and Fig. 1b): D_{ad} (measuring the closeness of C α packing at the core hydrophobic interface), D_{AS} (measuring the axial staggering between two Tpm chains) and D_{\perp} (measuring the lateral separation between two Tpm chains). We calculated both average (AVE) and standard deviation (SD) of the above parameters based on the last 10 ns of MD trajectories for both WT and Tpm mutants (see Fig. 2 and Fig S1-11 in the Supporting Information). The SD values are particularly informative in assessing the local flexibility/fluctuations of the Tpm coiled-coil. A peak in SD indicates elevated fluctuations

near a coiled-coil core residue at *a/d* position, which may be affected by a mutation at a nearby or distant site (see Fig. 2).

As found in Zheng et al. (2013), both the WT and the mutants exhibit six valleys (i.e. local minima) in the average of D_{ad} and D_{\perp} corresponding to six Ala clusters [named ALA1-ALA6, see Minakata et al. (2008)] centered at six core Ala residues (A22, A78, A120, A155, A183, and A239) (see Fig. 2 and Fig S1-11 in the Supporting Information). This is consistent with the close packing of the coiled-coil near the Ala clusters, which are robustly preserved despite point mutations or isoform differences. The above features were also observed in the crystal structures of Tpm (Zheng et al. 2013), which support the validity of the above MD-based local flexibility analysis.

As found in Zheng et al. (2013), the SD of D_{ad} and D_{AS} exhibit seven pronounced peaks, six of which align well with the six Ala clusters (see Fig. 2 and Fig S1-11 in the Supporting Information). In addition, a 7th peak is near a destabilizing core residue E218 (Minakata et al. 2008), and another destabilizing core residue D137 (Sumida et al. 2008) corresponds to a minor peak next to ALA3 (see Fig. 2 and Fig S1-11 in the Supporting Information). The SD profile of D_{ad} and D_{AS} largely overlap between WT and mutants, except for local differences attributed to the effect of mutations on the local flexibility of Tpm (both near the mutation site and in distant regions). By calculating the differences between the WT and mutant SD profiles, we can identify regions with local flexibility affected by a mutation (for details, see Fig. 2 and Fig S1-11 in the Supporting Information). Depending on the distance between the affected regions and the mutation site, we can distinguish between local and long-range effects of a mutation (for example, see Fig. 2).

As found in Zheng et al. (2013), the SD of D_{\perp} shows two peaks at the destabilizing core residues D137 and E218 (see Fig. 2 and Fig S1-11 in the Supporting Information). The heights of these two peaks vary between WT and some mutants, suggesting that the flexibility of these destabilizing regions is sensitive to mutations. For example, the D137L mutation greatly reduced the local flexibility near D137 (see Fig S5 in the Supporting Information).

To check the robustness of our analysis of D_{AS} and D_{\perp} , we also calculated two alternative parameters for measuring the axial staggering (denoted AS) and coiled-coil diameter by using the CCbends program (Brown 2010). Indeed, the profiles of AS and diameter are similar to that of D_{AS} and D_{\perp} , respectively (see Fig. 2 and Fig S1-11 in the Supporting Information).

In sum, we calculated the local flexibility parameters to directly probe the dynamics of the core residues in the Tpm coiled coil based on MD simulations, which exhibit robust and pronounced features that correlate well with the

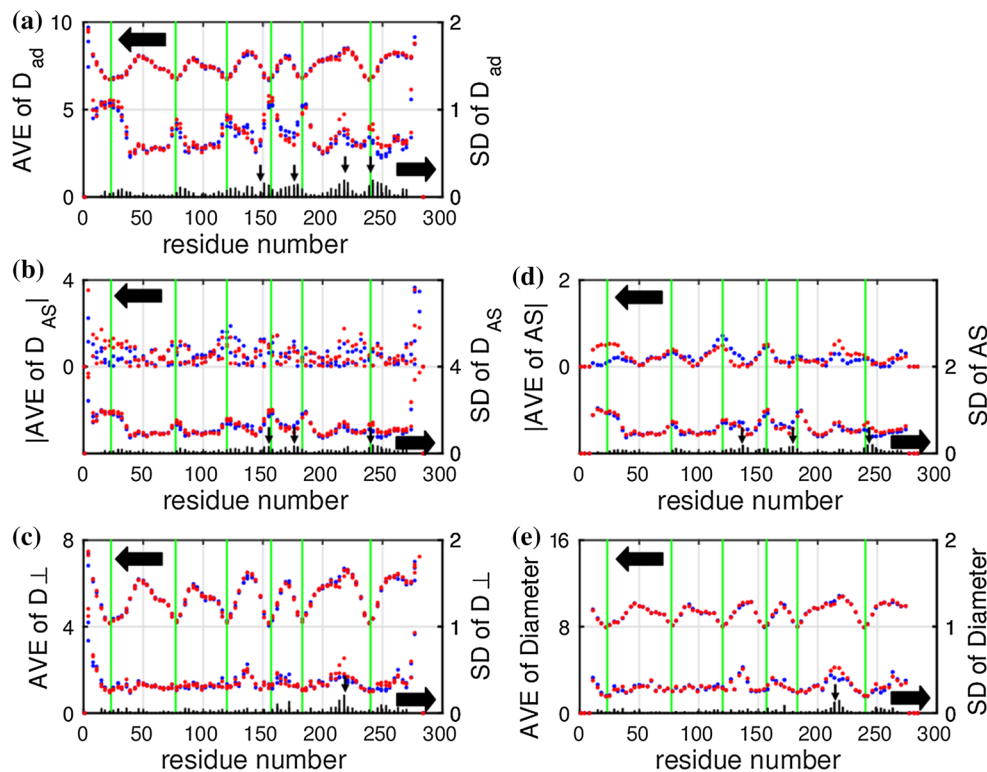


Fig. 2 Results of local flexibility analysis of the D175N mutant on F-actin in comparison with the WT Tpm using the following parameters: **a** D_{ad} , **b** D_{AS} , **c** D_{\perp} , **d** AS, **e** diameter. The average (AVE) and standard deviation (SD) of the above parameters as a function of ad residue positions of Tpm are shown as points (colored blue for the WT and red for the mutant). The data points for AVE (SD) are shown in the upper (lower) half of each panel as indicated by the block arrows. The green vertical lines mark the center positions of six Ala clusters (A22, A78, A120, A155, A183, and A239). The black

dashes give the SD differences between the WT and the mutant Tpm. Regions with pronounced SD differences are marked by arrows (e.g., near ALA4, ALA5, ALA6, and E218). This mutation caused both local changes (near ALA4 and ALA5) and long-range changes (near ALA6 and E218) in flexibility. The standard error for AVE and SD is $<0.03 \text{ \AA}$. We have verified the robustness of the observed small WT-mutant differences using different subsets of trajectories and different time windows. (Color figure online)

positions of six Ala clusters and two destabilizing residues (D137 and E218). In contrast, other flexibility parameters [such as Z-displacement, local curvature, local bending angle, see Li et al. (2010c) and Zheng et al. (2013)] depend on both core residues and neighboring residues, and do not correlate well with the locally destabilizing regions. By analyzing how the above features change between WT and mutants, we can obtain detailed information on how specific mutations perturb the flexibility of nearby and distant regions including those locally destabilizing regions (see below).

Analysis of Tpm movement over the surface of F-actin

In the three-state steric blocking model (McKillop and Geeves 1993; Vibert et al. 1997), Tpm is thought to move azimuthally over the F-actin surface from the peripheral blocked position in the absence of Ca^{2+} to the closed position, and then to the open position toward the

center of the groove of the helical F-actin in the presence of Ca^{2+} and strong-binding myosin heads. The initial model of Tpm used in our simulation is near the blocked position, although it was originally thought to represent the closed position (Li et al. 2011). To understand how Tpm mutations affect the above movements, we analyzed how the periods P2–P6 of WT and mutant Tpm move relative to the blocked and open position during the MD simulations. Following (Zheng et al. 2013), to measure the distances between Tpm and the blocked and open position (denoted as D_B and D_O , where D_B was named D_C in our previous MD study (Zheng et al. 2013)), we calculated the minimal $C\alpha$ – $C\alpha$ distances between Tpm and two representative residues (D25 and P307, see Fig. 1a) on five actin subunits in contact with the periods P2–P6 of Tpm. Residues D25 and P307 are close to Tpm at the blocked and open position, respectively (Zheng et al. 2013). We averaged the minimal distances from Tpm to D25 and P307 (corresponding to D_B and D_O) over the last 10 ns of MD

simulations. Then we subtracted the values of D_B and D_O as calculated for the initial model (Li et al. 2011) to obtain the changes in D_B and D_O during the MD simulations (denoted as δD_B and δD_O , see Table 2): a positive δD_B indicates that a Tpm period moves away from the blocked position, and a negative δD_O indicates that a Tpm period moves toward the open position.

For WT Tpm, the periods P2–P6 fluctuate variably near the blocked position ($-0.6 \text{ \AA} \leq \delta D_B \leq 1.7 \text{ \AA}$, see Table 2) while shifting close to the open position ($-3.5 \text{ \AA} \leq \delta D_O \leq -1.8 \text{ \AA}$, see Table 2). The observation of greater magnitude of δD_O than δD_B is partly due to dynamic fluctuations of both Tpm and F-actin allowing them to move closer to each other than in the initial model. While P4 undergoes the largest shift away from the blocked position (with average of $\delta D_B \sim 1.7 \text{ \AA}$, see Table 2), P5 shows the greatest variation in δD_B (with SD of $\delta D_B \sim 2.2 \text{ \AA}$, see Table 2). The finding of large variations in δD_B and δD_O between different periods indicates that Tpm fluctuates on F-actin with little cooperativity between the periods within the time scale of our

simulations. The mutants also exhibit large period-to-period variations in δD_B and δD_O that differ from the WT (and between the mutants) and may be attributed to either local or long-range effect of mutations. For example, the E54K and V95A mutant show a larger shift of P5 than the WT as a result of a mutation at a distant site in P2 and P3 (long-range effect), while the E180G mutant shows a larger shift of P5 than the WT as a result of a mutation in P5 itself (local effect). To focus on the overall shift of Tpm on F-actin and eliminate period-to-period variations, we averaged δD_B and δD_O over periods P2–P6. The average δD_B values are relatively small (between -0.1 and 0.6 \AA), which result from partial cancelation of positive and negative δD_B of different periods. The WT Tpm moves little (with average $\delta D_B \sim 0.1 \text{ \AA}$) relative to the blocked position. In contrast, most Tpm mutants exhibit larger movement relative to the blocked position (see Fig. 3), which correlates well with the Tpm–F-actin binding energy (with Pearson correlation = 0.78, see below). Interestingly, only the non-polar contribution (but not the electrostatic contribution) to binding energy correlates positively with the

Table 2 Results for analysis of Tpm movement relative to F-actin involving periods P2–P6 of Tpm

Period-actin	Average (SD) of δD_B , δD_O (Å)									
	WT		E54K		E62Q		A63V		K70T	
P2-AC15	-0.3 (1.6)	-3.0 (1.6)	0.8 (1.7)	-1.7 (1.3)	1.6 (1.5)	-1.6 (2.6)	1.3 (1.7)	-3.1 (1.8)	0.3 (1.8)	-2.7 (2.6)
P3-AC13	-0.3 (1.8)	-3.5 (1.1)	-0.5 (1.7)	-3.5 (1.1)	-0.2 (2.0)	-3.1 (1.6)	-0.5 (1.8)	-3.3 (1.1)	-0.7 (1.8)	-2.8 (1.4)
P4-AC11	1.7 (0.7)	-2.6 (1.2)	1.6 (0.9)	-1.7 (1.4)	1.7 (0.8)	-1.8 (3.2)	1.4 (0.7)	-2.2 (1.2)	1.8 (0.5)	-3.1 (1.5)
P5-AC09	-0.0 (2.2)	-2.2 (1.8)	1.5 (1.4)	-2.9 (1.6)	0.0 (1.8)	-1.9 (1.7)	0.0 (2.1)	-1.6 (1.4)	0.3 (1.2)	-1.1 (1.6)
P6-AC07	-0.6 (1.2)	-1.8 (1.6)	-0.4 (1.4)	-1.6 (1.5)	-1.2 (1.7)	-2.3 (1.6)	-1.1 (1.3)	-2.4 (1.2)	-0.2 (1.6)	-2.7 (1.4)
Average ^a	0.1	-2.6	0.6	-2.3	0.4	-2.1	0.2	-2.5	0.3	-2.5
	V95A		D175N		E180G		L185R		E192K	
P2-AC15	0.7 (1.7)	-2.9 (1.6)	0.8 (1.9)	-3.3 (1.9)	0.6 (1.6)	-3.1 (1.5)	-0.5 (2.0)	-2.2 (1.2)	0.1 (1.5)	-2.5 (2.0)
P3-AC13	0.1 (2.2)	-3.3 (1.8)	-0.1 (2.0)	-3.3 (1.6)	-1.4 (1.8)	-2.3 (1.2)	-1.0 (1.7)	-3.5 (1.2)	0.4 (1.7)	-3.0 (1.2)
P4-AC11	1.4 (0.8)	-2.7 (1.3)	2.1 (0.9)	-2.8 (1.7)	1.9 (0.9)	-2.1 (1.5)	1.5 (0.7)	-2.4 (1.1)	2.0 (1.2)	-2.8 (1.7)
P5-AC09	1.2 (1.7)	-1.8 (2.2)	0.6 (1.6)	-2.2 (1.4)	1.5 (1.4)	-1.8 (1.0)	0.7 (1.8)	-1.7 (1.6)	0.6 (1.4)	-2.2 (1.4)
P6-AC07	-1.3 (2.0)	-1.9 (1.5)	-1.0 (1.9)	-2.5 (2.0)	-1.4 (1.7)	-2.5 (1.9)	-1.1 (1.4)	-2.2 (1.6)	-0.3 (1.3)	-1.8 (2.2)
Average	0.4	-2.5	0.5	-2.8	0.2	-2.4	-0.1	-2.4	0.6	-2.5
	D137L		$\alpha\beta$		$\beta\alpha$					
P2-AC15	0.8 (1.5)	-2.7 (2.0)	0.8 (1.1)	-1.9 (2.2)	1.6 (1.5)	-3.3 (1.6)				
P3-AC13	-1.4 (1.9)	-2.8 (1.1)	-0.3 (1.8)	-2.9 (1.2)	-0.1 (2.0)	-3.3 (1.3)				
P4-AC11	1.7 (0.7)	-2.5 (1.2)	1.9 (1.2)	-2.9 (1.3)	1.7 (1.0)	-2.0 (1.1)				
P5-AC09	0.3 (1.7)	-2.6 (1.2)	1.2 (1.5)	-2.5 (1.3)	0.5 (1.4)	-1.5 (1.5)				
P6-AC07	-0.9 (1.8)	-1.5 (1.4)	-2.1 (1.0)	-1.6 (1.2)	-1.4 (1.4)	-2.6 (1.2)				
Average	0.1	-2.4	0.3	-2.4	0.4	-2.5				

^a Standard error of the average is $\sim 0.01 \text{ \AA}$. We have verified the robustness of the observed small WT-mutant differences in average δD_B using different subsets of trajectories and different time windows

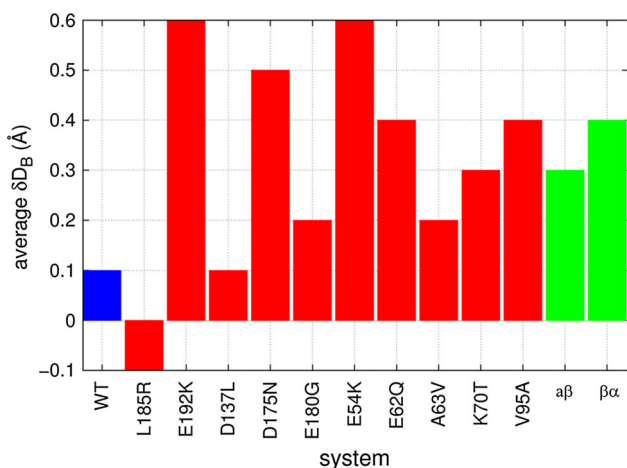


Fig. 3 Results of the analysis of Tpm movement relative to the blocked position on the F-actin surface: the average δD_B for the WT Tpm (blue), ten Tpm mutants (red), and two Tpm heterodimers (green). The standard error for the average δD_B is ~ 0.01 Å. See Table 2 for further details. (Color figure online)

average δD_B (with Pearson correlation = 0.88). Therefore, the Tpm mutants that move further away from the blocked position bind more weakly with F-actin. As a result, mutations that weaken Tpm–F-actin binding at the blocked position could favor the blocked-to-closed movement of Tpm and thereby the activation of thin filaments (see “Discussion of Tpm mutations” section).

Binding calculation between Tpm and actin subunits

Following (Zheng et al. 2013), we performed binding calculation between Tpm and F-actin, which take into account both electrostatic and non-polar contributions to Tpm–F-actin binding (see “Methods” section). This calculation cannot yield results comparable to experimental binding measurements for the lack of entropic contribution to binding, the missing head-to-tail interactions in the overlap regions of Tpm, and the loss of cooperativity due to binding of multiple Tpm under experimental conditions. Despite the above caveats, this binding calculation allows us to dissect the contributions of each Tpm period to binding, and predict the changes between WT and mutant Tpm (with the entropy term largely cancelled out). In the binding calculation, based on the last 10 ns of MD simulations, we calculated and averaged the binding free energy ΔG between Tpm and each of five actin subunits interacting with the periods P2–P6 of Tpm (see “Methods” section and Fig. 1a). This protocol was established in our previous studies of the complex between kinesin motor and tubulins (Li and Zheng 2011, 2012).

For both WT and mutant Tpm, the total ΔG (i.e. sum of ΔG over all five actin subunits) varies between -11.6 and -13 kcal/mol (see Fig. 4; Table 3), with most mutants and

the $\alpha\beta/\beta\alpha$ -Tpm heterodimer showing weaker (less negative) ΔG (except A63V, D137L, and L185R). As found in Zheng et al. (2013), for both WT and mutants, the non-polar contribution is as significant as the electrostatic contribution (even after weighting by α and β), highlighting the importance of forming extensive Tpm–actin atomic contacts to binding (involving both nonpolar and charged residues). While the electrostatic interactions between actin and Tpm are considered to predominate (Li et al. 2011; Lorenz et al. 1995), we note that the Phillips model of quasi-equivalent actin-binding sites includes charged as well as non-polar residues (Phillips 1986). Barua et al. (2013) provided experimental support for the contribution of both charged and hydrophobic interactions to actin binding (Barua et al. 2013). The cold sensitive binding of Tpm to actin also supports the hydrophobic effect (Hitchcock-DeGregori and Singh 2010).

The total ΔG values of the mutants and WT do not seem to correlate with the overall Tpm flexibility as given by $\langle \text{RMSF} \rangle_{\text{Tpm or F-actin}}$ (with Pearson correlation < 0.2). Interestingly, we found some correlation between PL and the electrostatic and non-polar contribution of ΔG (with Pearson correlation = -0.42 and 0.52 , respectively), suggesting that the less curved Tpm mutants (such as E54K and E192K) tend to exhibit weaker non-polar interactions while the more curved mutants (such as E62Q) may show weaker electrostatic interactions between Tpm and F-actin.

Discussion of Tpm mutations

Here we will discuss individual Tpm mutations and heterodimers by correlating the results of flexibility and

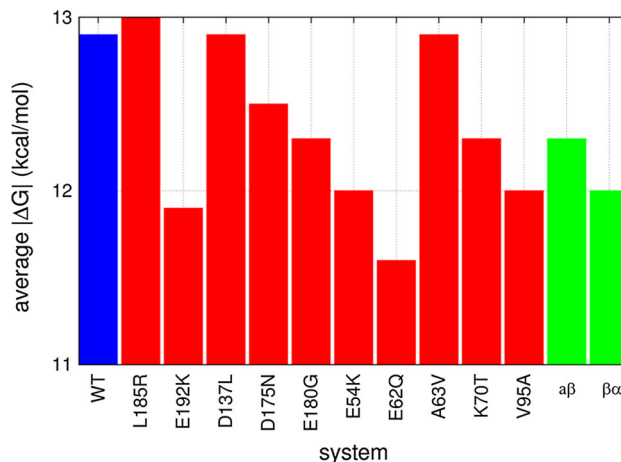


Fig. 4 Results of the Tpm–F-actin binding calculation: the average $|\Delta G|$ for the WT Tpm (blue), ten Tpm mutants (red), and two Tpm heterodimers (green). The standard error for the average ΔG is only ~ 0.1 kcal/mol, so the observed small differences in ΔG between WT and mutants are statistically significant. See Table 3 for further details. (Color figure online)

Table 3 Results of Tpm–F-actin binding calculations involving periods P2–P6 of Tpm

Period-actin	Average (SD) of $\Delta G = 0.08E_{vdW} + 0.12\Delta E_{elec}$, E_{vdW} , ΔE_{elec} (kcal/mol)											
	WT			E54K			E62Q			A63V		
P2-AC15	-2.6 (0.5)	-17.9 (8.3)	-9.5 (3.1)	-2.3 (0.6)	-9.4 (7.7)	-12.6 (2.9)	-1.5 (0.6)	-10.6 (5.9)	-5.9 (2.8)	-2.4 (0.5)	-15.4 (6.5)	-9.9 (3.2)
P3-AC13	-2.7 (0.7)	-16.3 (8.8)	-11.9 (4.2)	-2.7 (0.8)	-18.0 (8.3)	-10.8 (3.5)	-2.5 (0.8)	-13.8 (10.8)	-11.6 (4.0)	-2.6 (0.6)	-17.7 (9.2)	-10.1 (3.6)
P4-AC11	-2.6 (0.5)	-12.4 (7.4)	-13.7 (3.1)	-2.4 (0.5)	-12.8 (7.5)	-11.8 (2.7)	-2.4 (0.7)	-13.3 (7.4)	-11.2 (3.5)	-2.5 (0.5)	-14.8 (7.3)	-11.3 (2.6)
P5-AC09	-2.8 (0.9)	-19.2 (9.2)	-10.5 (4.2)	-2.2 (0.6)	-14.3 (7.2)	-9.1 (3.4)	-2.8 (0.9)	-20.7 (9.8)	-9.2 (3.5)	-2.8 (0.9)	-19.5 (9.7)	-10.2 (5.1)
P6-AC07	-2.1 (0.5)	-17.0 (6.6)	-6.5 (2.3)	-2.3 (0.5)	-17.1 (6.0)	-8.0 (3.2)	-2.4 (0.6)	-19.5 (8.4)	-6.8 (3.0)	-2.5 (0.6)	-18.8 (7.2)	-8.1 (3.4)
Sum (SE ^a)	-12.9 (0.1)	-82.9 (0.6)	-52.2 (0.2)	-12.0 (0.1)	-71.6 (0.8)	-52.3 (0.3)	-11.6 (0.1)	-78.0 (0.6)	-44.6 (0.3)	-12.9 (0.1)	-86.3 (0.7)	-49.7 (0.4)
	K70T			V95A			D175N					
P2-AC15	-2.6 (0.8)	-17.1 (9.5)	-10.0 (3.3)	-2.4 (0.7)	-16.6 (7.9)	-9.3 (2.9)	-2.6 (0.7)	-17.3 (11.5)	-9.7 (4.0)			
P3-AC13	-2.5 (0.8)	-16.5 (11.6)	-10.0 (3.4)	-2.5 (0.7)	-15.6 (9.4)	-10.1 (5.0)	-2.4 (0.6)	-15.3 (7.6)	-10.1 (2.8)			
P4-AC11	-2.5 (0.6)	-16.2 (7.6)	-10.1 (2.4)	-2.7 (0.5)	-12.9 (7.0)	-13.6 (2.7)	-2.5 (0.6)	-14.8 (7.6)	-11.1 (3.2)			
P5-AC09	-2.6 (0.8)	-16.0 (8.2)	-11.1 (4.3)	-2.1 (0.6)	-15.4 (7.3)	-7.3 (3.8)	-2.9 (0.8)	-18.4 (8.0)	-11.7 (3.8)			
P6-AC07	-2.1 (0.5)	-14.0 (8.0)	-8.5 (3.3)	-2.3 (0.6)	-18.1 (7.4)	-7.4 (2.7)	-2.1 (0.6)	-15.9 (7.8)	-7.1 (2.6)			
Sum (SE ^a)	-12.3 (0.0)	-79.8 (0.6)	-49.6 (0.3)	-12.0 (0.1)	-78.5 (0.8)	-47.7 (0.3)	-12.5 (0.0)	-81.9 (0.6)	-49.8 (0.3)			
	E180G			L185R			E192K					
P2-AC15	-2.5 (0.5)	-15.2 (6.3)	-11.0 (3.8)	-2.7 (0.8)	-19.9 (9.8)	-9.2 (3.2)	-2.3 (0.6)	-13.9 (8.2)	-10.0 (4.0)			
P3-AC13	-2.9 (0.8)	-21.7 (10.7)	-9.4 (3.5)	-2.8 (0.5)	-18.6 (8.0)	-10.7 (2.9)	-2.3 (0.6)	-13.0 (7.7)	-10.5 (3.6)			
P4-AC11	-2.4 (0.6)	-13.5 (7.0)	-11.0 (2.9)	-2.6 (0.5)	-15.2 (7.8)	-11.8 (4.2)	-2.7 (0.6)	-13.9 (8.5)	-13.3 (3.8)			
P5-AC09	-2.2 (0.7)	-14.9 (8.2)	-8.5 (4.3)	-2.8 (0.7)	-20.2 (9.7)	-10.0 (3.5)	-2.6 (0.7)	-15.7 (6.7)	-10.9 (4.4)			
P6-AC07	-2.3 (0.6)	-20.2 (7.1)	-6.0 (2.7)	-2.1 (0.6)	-15.9 (6.5)	-7.0 (3.4)	-2.0 (0.5)	-15.0 (7.4)	-6.6 (2.5)			
sum (SE)	-12.3 (0.1)	-85.5 (0.7)	-45.9 (0.3)	-13.0 (0.1)	-89.7 (1.1)	-48.7 (0.4)	-11.9 (0.1)	-71.6 (0.7)	-51.2 (0.4)			
	D137L			$\alpha\beta$			$\beta\alpha$					
P2-AC15	-2.3 (0.6)	-12.4 (7.2)	-10.7 (3.0)	-2.1 (0.5)	-11.3 (6.8)	-9.8 (2.9)	-2.2 (0.5)	-12.2 (7.9)	-10.3 (3.1)			
P3-AC13	-2.9 (0.9)	-18.9 (11.8)	-11.9 (3.7)	-2.3 (0.6)	-16.1 (7.6)	-8.4 (3.9)	-2.5 (0.5)	-15.7 (6.6)	-10.1 (3.8)			
P4-AC11	-2.6 (0.6)	-15.5 (7.2)	-11.3 (3.1)	-2.8 (0.5)	-19.1 (7.9)	-10.7 (2.8)	-2.6 (0.4)	-12.9 (6.6)	-13.2 (3.5)			
P5-AC09	-3.0 (0.6)	-21.5 (7.2)	-10.7 (4.3)	-2.6 (0.9)	-17.8 (6.7)	-9.5 (5.4)	-2.3 (0.8)	-11.8 (7.9)	-11.7 (4.6)			
P6-AC07	-2.1 (0.7)	-14.8 (8.8)	-7.5 (2.8)	-2.5 (0.6)	-19.8 (6.9)	-7.6 (3.8)	-2.4 (0.5)	-19.2 (7.4)	-7.1 (2.8)			
sum (SE)	-12.9 (0.1)	-83.1 (0.9)	-52.2 (0.4)	-12.3 (0.1)	-84.1 (0.7)	-46.1 (0.4)	-12.0 (0.1)	-71.8 (0.7)	-52.4 (0.4)			

^a Standard error (SE) for ΔG summed over P2–P6

binding analysis with experimental data and clinical phenotype. While the mutational effects on flexibility varies between mutants (with increase or decrease in RMSF and PL), a majority of them exhibited weaker actin binding (except for L185R, D137L and A63V), which is consistent with easier activation of the blocked-to-closed transition. Additionally, each mutation causes both local and long-range effects on Tpm flexibility consistent with long-range coupling in Tpm.

The E54K mutant (a DCM-causing mutation) exhibits much weaker binding with F-actin than the WT (see Fig. 4) due to weaker actin binding in periods P2, P4, and P5 (see Table 3), which agrees with the finding that the E54K mutant showed diminished actin-binding affinity in the off state (i.e., in the absence of troponin and myosin) (Mirza et al. 2007). E54 is located in a consensus actin-binding site

of Tpm (Phillips 1986; Phillips et al. 1986), and was found to contribute to actin binding in our previous study (Zheng et al. 2013). E54 is at the *e* position of the heptad repeat and can form a salt bridge with K49 on the other Tpm chain, so it plays a role in stabilizing the Tpm coiled coil structure. Indeed, the E54K mutation was found to destabilize some part and stabilize another part of the Tpm coiled coil (Mirza et al. 2007). Our flexibility analysis found that the E54K mutation reduces the RMSF, increases the PL (see Table 1), and alters local flexibility in distant regions [near D137, E218, and ALA5 (the 5th Ala cluster) in P5, see Fig S6]. Functionally the E54K mutant was shown to exhibit impaired inhibition of the actomyosin ATPase activity in myofilament at low Ca^{2+} (Chang et al. 2005, 2014), which is consistent with our finding of weakened actin binding in the blocked state.

The E62Q mutant exhibits much weaker binding with F-actin than the WT (see Fig. 4) due to weaker actin binding in periods P2, P3, and P4 (see Table 3). E62 is at a consensus actin-binding site of Tpm (Phillips 1986; Phillips et al. 1986), and was found to contribute to actin binding in our previous study (Zheng et al. 2013). A recent computational energy-landscape study also found the E62Q mutation weakens actin–Tpm interaction (Orzechowski et al. 2014). However, this mutation did not seem to change actin-binding affinity in a co-sedimentation study (Gupte et al. 2015) although further studies are needed to confirm this finding. Since E62 is at the *f* position of the heptad repeat, the E62Q mutation is not expected to destabilize the Tpm coiled coil structure which is consistent with the finding of intact thermal stability (Chang et al. 2014). Our flexibility analysis of E62Q found increased RMSF, decreased PL (see Table 1), and altered local flexibility of distant regions (near ALA1, ALA5, ALA6, and E218, see Fig S1 in the Supporting Information). Clinically the E62Q mutation is associated with a malignant form of HCM (Jongbloed et al. 2003) with impaired inhibition of actomyosin ATPase activity (Chang et al. 2014). This functional defect is consistent with our finding of weakened actin binding in the blocked state.

The A63V mutant exhibits WT actin binding (see Fig. 4) due to weaker actin binding in P2 compensated by stronger actin binding in P6 (see Table 3). A63 is not directly involved in actin binding or stabilization of the Tpm coiled coil. Structural analysis showed the A63V mutant with decreased thermal stability (Heller et al. 2003), which agrees with our flexibility analysis that found increased RMSF and decreased PL than the WT (see Table 1) and altered local flexibility in distant regions (near ALA1, ALA3, ALA4, ALA6, and E218, see Fig S2 in the Supporting Information). Clinically, this mutant showed moderate phenotype (Nakajima-Taniguchi et al. 1995), with slower relaxation and higher thin-filament Ca^{2+} sensitivity (Michele et al. 2002). This is consistent with our finding of little perturbation to actin binding.

The K70T mutant exhibits weaker actin binding than the WT (see Fig. 4) due to weaker actin binding in periods P3 and P5 (see Table 3). Since K70 is at the *g* position of the heptad repeat (forming a salt-bridge with E75 on the other Tpm chain), it is involved in stabilizing the Tpm coiled coil structure. Indeed, the K70T mutation was found to severely destabilize the Tpm coiled coil leading to decreased thermal stability (Heller et al. 2003; Hilario et al. 2004). Our flexibility analysis found increased RMSF and PL than the WT (see Table 1) and altered local flexibility near ALA1, ALA3, ALA5, and E218 (see Fig S3 in the Supporting Information). Clinically, K70T is one of the most deleterious HCM mutations with individuals carrying this mutation having a high incidence of sudden death

(Nakajima-Taniguchi et al. 1995) (Yamauchi-Takahara et al. 1996). This is consistent with our finding of large mutational effects on Tpm's flexibility and actin binding in the blocked state.

The V95A mutant exhibits much weaker actin binding than the WT (see Fig. 4) due to weaker actin binding in periods P2, P3, and P5 (see Table 3). V95 is at the *d* position of the heptad repeat, so it is involved in stabilizing the Tpm coiled coil structure. As expected, the V95A mutation was found to destabilize the Tpm coiled coil structure (Wang et al. 2011). Our flexibility analysis of V95A found decreased RMSF, increased PL (see Table 1), and altered local flexibility near ALA2, ALA4, and ALA5 (featuring anomalously high flexibility near ALA2, see Fig S4 in the Supporting Information). Clinically the V95A mutation causes severe symptoms and poor prognosis in patients (Karibe et al. 2001), with significant increase in the Ca^{2+} sensitivity in thin filament (Bai et al. 2013) and in vitro (Wang et al. 2011). This is consistent with our finding of large mutational effects on Tpm's local flexibility and actin binding.

The D137L mutant is a synthetic mutant designed to test the importance of this unusual conserved Asp for Tpm folding and function. This mutation does not affect actin binding (see Fig. 4) due to weaker actin binding in P2 compensated by stronger binding in P3 and P5 (see Table 3). In agreement with our finding, this mutation was shown not to alter Tpm–actin binding (Sumida et al. 2008). The conserved D137 is at a *d* position within the hydrophobic core of the Tpm coiled coil, so it is thought to destabilize the coiled coil and impart flexibility to the Tpm, and the D137L mutation would stabilize the Tpm structure. Indeed, the D137L mutant was found to have higher thermal stability than the WT, which implies decreased flexibility (Yar et al. 2013). The D137L mutation stabilizes not only the middle region of Tpm [e.g., near R133 (Sumida et al. 2008)], but also the other parts of Tpm including the N- and C-terminal parts (Matyushenko et al. 2015). In agreement with these findings, we found increased PL (see Table 1), decreased local flexibility near D137, ALA1, and ALA5, and increased local flexibility near ALA2 and E218 (see Fig S5 in the Supporting Information). Our finding differs from a previous simulation study of the D137L mutant that found an increase in global flexibility and large structural change in actin-free Tpm (Moore et al. 2011), suggesting that actin binding might alter the properties of the D137L mutant.

The D175N mutant exhibits slightly weaker actin binding than the WT (see Fig. 4) due to weaker actin binding in period P3 (see Table 3). D175 was found to contribute to actin binding in our previous study (Zheng et al. 2013). Experimentally, the D175N mutant was shown to bind less strongly to F-actin than the WT in several

binding studies (Boussouf et al. 2007; Janco et al. 2012; Kremneva et al. 2004) although the actin-binding affinity was un-affected in other studies (Bing et al. 1997; Golitsina et al. 1997, 1999). D175 is at the *g* position of the heptad repeat, so it is likely involved in stabilizing the Tpm coiled coil structure. Indeed, the D175N mutation increases the local flexibility of Tpm (Ly and Lehrer 2012) without changing the overall thermal stability (Kremneva et al. 2004). Our flexibility analysis found increased RMSF than the WT (see Table 1) and altered local flexibility near ALA4, ALA5, ALA6, and E218 (see Fig. 2). Clinically the D175N mutation causes only mild hypertrophic phenotype (Bai et al. 2013; Muthuchamy et al. 1999), which is consistent with our finding of moderate mutational effect on Tpm–actin binding.

The E180G mutant exhibits weaker actin binding (see Fig. 4) than the WT due to weaker actin binding in P4 and P5 (see Table 3), in agreement with experimental binding measurements (Bing et al. 1997; Boussouf et al. 2007; Golitsina et al. 1997, 1999; Janco et al. 2012; Kremneva et al. 2004). E180 is at the *e* position of the heptad repeat (forming a salt bridge with R182 of another Tpm chain), so it is involved in stabilizing the Tpm coiled coil structure. As expected, the E180G mutation was shown to cause greater structural disorder (Wang et al. 2011), decreased thermal stability in the C-terminal part (Kremneva et al. 2004), increased local flexibility [near R133 and K233 (Ly and Lehrer 2012)], and decreased PL (Loong et al. 2012a, b). Surprisingly, our flexibility analysis found lower RMSF and higher PL than the WT (see Table 1) and altered local flexibility near D137, ALA5, and E218 (see Fig S7 in the Supporting Information). It is possible that the E180G mutation has opposite effects on free and actin-bound Tpm. Clinically the E180G mutation leads to severe cardiac hypertrophy and death in mice with impaired relaxation and increased Ca^{2+} sensitivity (Prabhakar et al. 2001). Our finding of greater perturbation to actin-Tpm binding (particularly in P5, see Table 3) by the E180G mutation than the D175N mutation is consistent with E180G causing more marked abnormalities than D175N. Beyond the scope of this study, other contributing factors to the E180G phenotype may involve Tpm–troponin interactions (Bing et al. 1997; Golitsina et al. 1997) and Tpm conformation in the open state (Golitsina et al. 1997).

The L185R mutant exhibits slightly stronger actin binding than WT (see Fig. 4) due to slightly stronger actin binding in periods P2 and P3 (see Table 3). L185 is at a consensus actin-binding site (Phillips 1986; Phillips et al. 1986), and was found to contribute to actin binding in our previous study (Zheng et al. 2013). A substitution by a basic residue may allow new electrostatic interactions to form with the negatively charged F-actin surface. In agreement with our calculation, a co-sedimentation

measurement of Tpm–actin binding showed a two-fold increase in affinity from the WT to L185R (Gupte et al. 2015). This mutation was found to increase the overall thermal stability of Tpm (Chang et al. 2014; Gupte et al. 2015). Indeed, our flexibility analysis found lower RMSF in L185R than the WT (see Table 1) and altered local flexibility near ALA1, ALA5, and E218 (see Fig S8 in the Supporting Information). Taken together, the above findings suggest that the HCM-causing mechanism of L185R mutation (e.g., higher Ca^{2+} sensitivity and impaired inhibition of actomyosin ATPase) cannot be explained by perturbation to the Tpm–actin interaction and flexibility in the blocked state and may involve modification of other properties like Tpm–troponin binding (Van Driest et al. 2002).

The E192K mutant exhibits much weaker actin binding than the WT (see Fig. 4) due to weaker actin binding in periods P2, P3 and P5 (see Table 3). E192 is at the *c* position of the heptad repeat, and was found to contribute to actin binding in our previous study (Zheng et al. 2013). Our flexibility analysis found decreased RMSF, increased PL (see Table 1), and increased local flexibility near ALA2, ALA3, and E218, and reduced flexibility near ALA1 and ALA4 (see Fig S9 in the Supporting Information). This mutation causes left ventricular noncompaction, but the underlying mechanism at the molecular level remains unclear (Bai et al. 2013). Our findings suggest that weakened actin-Tpm binding in the blocked state may contribute to the disease phenotype of E192K mutant.

Finally, we analyzed the $\alpha\beta$ -Tpm and $\beta\alpha$ -Tpm heterodimers, where chain B or A of the $\alpha\alpha$ -Tpm homodimer is replaced by β -Tpm (see Fig. 1a). Both $\alpha\beta$ -Tpm and $\beta\alpha$ -Tpm exhibit weaker actin binding (see Table 3). The $\alpha\alpha \rightarrow \alpha\beta$ isoform change, which sequentially alters the actin-binding sites in periods P2, P4, and P6 of chain B (see Fig. 1a), led to weaker actin binding in P2, P3, and P5 partially compensated by stronger actin binding in P4 and P6; the $\alpha\alpha \rightarrow \beta\alpha$ isoform change, which sequentially alters the actin-binding sites in periods P3 and P5 of chain A (see Fig. 1a), led to weaker actin binding in P2, P3, and P5 partially compensated by stronger actin binding in P6. The $\beta\alpha$ -Tpm shows weaker actin binding than the $\alpha\beta$ -Tpm primarily due to weaker actin binding in periods P4 and P5 (see Table 3). Consistent with our calculation, the $\alpha\beta$ heterodimer of Tpm was found to have weaker actin-binding affinity than the $\alpha\alpha$ and $\beta\beta$ homodimers of Tpm (Kalyva et al. 2012). The thermal stability of $\alpha\beta/\beta\alpha$ -Tpm is weaker than $\alpha\alpha$ -Tpm (Kalyva et al. 2012), suggesting higher flexibility of the hetero-dimer of Tpm. Indeed, we found that both the $\alpha\beta$ - and the $\beta\alpha$ -Tpm dimers had greater RMSF (see Table 1) accompanied by altered local flexibility (near ALA1-5, D137 and E218, see Fig S10 and S11 in the Supporting Information).

Sequence alignment reveals 40 amino-acid substitutions between α -Tpm and β -Tpm, most of which preserve the chemical property of amino acids (see Table S1 in the Supporting Information). The following substitutions involve those residues identified to contribute to actin binding in our previous study (Zheng et al. 2013): V44Q and D58E of P2, Q135M of P4, S174G of P5, and Q216T of P6. They may directly affect actin-binding affinity. The following substitutions chemically perturb the *a/d* positions critical to the stability of Tpm coiled coil structure: S36C and L43Q of P2, A158S of P4, A179S and S186A of P5. They may affect the local flexibility of Tpm and indirectly affect the actin-binding affinity. Notably, P5 has more α -to- β substitutions than any other periods (see Table S1), which might explain our findings that the $\beta\alpha$ -Tpm is perturbed more than the $\alpha\beta$ -Tpm (see Tables 1, 2, 3). Future studies will be needed to elucidate the effects of these individual substitutions.

Conclusion

Based on extensive MD simulations of various Tpm mutants and heterodimers in complex with F-actin, we have explored key dynamic and energetic properties of Tpm near the blocked position which are relevant to the regulatory function of Tpm. Our simulation and analysis offer detailed information on how Tpm mutations (and isoform differences) affect its overall and local flexibility and its interactions with F-actin. A common feature of these Tpm mutations is the coexistence of both local and long-range changes to the flexibility and actin binding (i.e., a point mutation affects the flexibility and actin-binding energy of distant regions). The existence of long-range couplings in Tpm is supported by previous studies [see Brown (2013)]. The mutational effects on Tpm–F-actin binding may be direct (with the mutated residue directly interacting with F-actin in E54K, E62Q, D175N, L185R, and E192K) or indirect (with the mutated residue involved in the flexibility or stability of Tpm in K70T, V95A, and E180G). While the direct effects can be readily assessed by inspecting the local interactions involving the mutated residue, the indirect long-range effects are more complex. Encouragingly, we found a significant correlation between actin-binding energy and Tpm's movement relative to the blocked position, which suggests a disease mechanism by which the HCM mutations weaken actin–Tpm binding in the blocked state and thereby enhancing the transition of Tpm from blocked to closed/open state. Intriguingly, E54K behaves similarly to the other HCM mutants even though it leads to the DCM disease phenotype. We also found opposite correlations between the persistent length of Tpm mutants and the electrostatic versus non-polar contribution

to the actin-binding energy, suggesting that a change in the global curvature and flexibility of Tpm mutants can weaken their electrostatic/non-polar interactions with F-actin in distinct manners.

In the future, we will perform mutational and binding experiments to test the computational predictions of the mutational effects on actin–Tpm binding in relation to HCM and DCM. Additionally, we will run new MD simulations to explore alternative Tpm positions as revealed by recent cryo-EM (Sousa et al. 2013; von der Ecken et al. 2015) and computational studies (Rynkiewicz et al. 2015), which were not explored by the current simulation due to limited computing resource.

Acknowledgments We thank funding support from American Heart Association (#14GRNT18980033) and National Science Foundation (#0952736) to WZ, and National Institutes of Health (GM093065) to SEHD and BB. We thank Dr. Lehman for sharing the EM-based model of Tpm–F-actin complex. The simulations were conducted using the supercomputing cluster of the Center for Computational Research at the University at Buffalo and the Biowulf cluster at the National Institutes of Health.

References

- Bai F, Wang L, Kawai M (2013) A study of tropomyosin's role in cardiac function and disease using thin-filament reconstituted myocardium. *J Muscle Res Cell Motil* 34:295–310. doi:[10.1007/s10974-013-9343-z](https://doi.org/10.1007/s10974-013-9343-z)
- Barua B, Pamula MC, Hitchcock-DeGregori SE (2011) Evolutionarily conserved surface residues constitute actin binding sites of tropomyosin. *Proc Natl Acad Sci USA* 108:10150–10155. doi:[10.1073/pnas.1101221108](https://doi.org/10.1073/pnas.1101221108)
- Barua B, Fagnant PM, Winkelmann DA, Trybus KM, Hitchcock-DeGregori SE (2013) A periodic pattern of evolutionarily-conserved basic and acidic residues constitutes the binding interface of actin–tropomyosin. *J Biol Chem* 288:9602–9609. doi:[10.1074/jbc.M113.451161](https://doi.org/10.1074/jbc.M113.451161)
- Behrmann E, Muller M, Penczek PA, Mannherz HG, Manstein DJ, Raunser S (2012) Structure of the rigor actin–tropomyosin–myosin complex. *Cell* 150:327–338. doi:[10.1016/j.cell.2012.05.037](https://doi.org/10.1016/j.cell.2012.05.037)
- Bing W, Redwood CS, Purcell IF, Esposito G, Watkins H, Marston SB (1997) Effects of two hypertrophic cardiomyopathy mutations in alpha-tropomyosin, Asp175Asn and Glu180Gly, on Ca²⁺ regulation of thin filament motility. *Biochem Biophys Res Commun* 236:760–764. doi:[10.1006/bbrc.1997.7045](https://doi.org/10.1006/bbrc.1997.7045)
- Boussouf SE, Maytum R, Jaquet K, Geeves MA (2007) Role of tropomyosin isoforms in the calcium sensitivity of striated muscle thin filaments. *J Muscle Res Cell Motil* 28:49–58. doi:[10.1007/s10974-007-9103-z](https://doi.org/10.1007/s10974-007-9103-z)
- Brooks BR, Bruccoleri RE, Olafson BD, States DJ, Swaminathan S, Karplus M (1983) Charmm—a program for macromolecular energy minimization, and dynamics calculations. *J Comput Chem* 4:187–217
- Brown JH (2010) How sequence directs bending in tropomyosin and other two-stranded alpha-helical coiled coils. *Protein Sci* 19:1366–1375. doi:[10.1002/pro.415](https://doi.org/10.1002/pro.415)
- Brown JH (2013) Deriving how far structural information is transmitted through parallel homodimeric coiled-coils: a

- correlation analysis of helical staggers. *Proteins* 81:635–643. doi:[10.1002/prot.24218](https://doi.org/10.1002/prot.24218)
- Brown JH et al (2001) Deciphering the design of the tropomyosin molecule. *Proc Natl Acad Sci USA* 98:8496–8501. doi:[10.1073/pnas.131219198](https://doi.org/10.1073/pnas.131219198)
- Brown JH, Zhou Z, Reshetnikova L, Robinson H, Yammani RD, Tobacman LS, Cohen C (2005) Structure of the mid-region of tropomyosin: bending and binding sites for actin. *Proc Natl Acad Sci USA* 102:18878–18883. doi:[10.1073/pnas.0509269102](https://doi.org/10.1073/pnas.0509269102)
- Caves LS, Evanseck JD, Karplus M (1998) Locally accessible conformations of proteins: multiple molecular dynamics simulations of crambin. *Protein Sci* 7:649–666. doi:[10.1002/pro.5560070314](https://doi.org/10.1002/pro.5560070314)
- Chang AN, Harada K, Ackerman MJ, Potter JD (2005) Functional consequences of hypertrophic and dilated cardiomyopathy-causing mutations in alpha-tropomyosin. *J Biol Chem* 280:34343–34349. doi:[10.1074/jbc.M505014200](https://doi.org/10.1074/jbc.M505014200)
- Chang AN, Greenfield NJ, Singh A, Potter JD, Pinto JR (2014) Structural and protein interaction effects of hypertrophic and dilated cardiomyopathic mutations in alpha-tropomyosin. *Front Physiol* 5:460. doi:[10.3389/fphys.2014.00460](https://doi.org/10.3389/fphys.2014.00460)
- Craig R, Lehman W (2001) Crossbridge and tropomyosin positions observed in native, interacting thick and thin filaments. *J Mol Biol* 311:1027–1036. doi:[10.1006/jmbi.2001.4897](https://doi.org/10.1006/jmbi.2001.4897)
- Deserno M, Holm C (1998) How to mesh up Ewald sums. I. A theoretical and numerical comparison of various particle mesh routines. *J Chem Phys* 109:7678–7693
- Eriksson MA, Roux B (2002) Modeling the structure of agitoxin in complex with the Shaker K⁺ channel: a computational approach based on experimental distance restraints extracted from thermodynamic mutant cycles. *Biophys J* 83:2595–2609. doi:[10.1016/S0006-3495\(02\)75270-3](https://doi.org/10.1016/S0006-3495(02)75270-3)
- Geeves MA, Hitchcock-DeGregori SE, Gunning PW (2015) A systematic nomenclature for mammalian tropomyosin isoforms. *J Muscle Res Cell Motil* 36:147–153. doi:[10.1007/s10974-014-9389-6](https://doi.org/10.1007/s10974-014-9389-6)
- Gilson MK, Honig BH (1986) The dielectric constant of a folded protein. *Biopolymers* 25:2097–2119. doi:[10.1002/bip.3602511106](https://doi.org/10.1002/bip.3602511106)
- Gilson MK, Honig BH (1988) Energetics of charge–charge interactions in proteins. *Proteins* 3:32–52. doi:[10.1002/prot.340030104](https://doi.org/10.1002/prot.340030104)
- Golitsina N et al (1997) Effects of two familial hypertrophic cardiomyopathy-causing mutations on alpha-tropomyosin structure and function. *Biochemistry* 36:4637–4642. doi:[10.1021/bi962970y](https://doi.org/10.1021/bi962970y)
- Golitsina N et al (1999) Effects of two familial hypertrophic cardiomyopathy-causing mutations on alpha-tropomyosin structure and function. *Biochemistry* 38:3850. doi:[10.1021/bi9950701](https://doi.org/10.1021/bi9950701)
- Gunning P (2008) Emerging issues for tropomyosin structure, regulation, function and pathology. *Adv Exp Med Biol* 644:293–298
- Gupte TM et al (2015) Mechanistic heterogeneity in contractile properties of alpha-tropomyosin (TPM1) mutants associated with inherited cardiomyopathies. *J Biol Chem* 290:7003–7015. doi:[10.1074/jbc.M114.596676](https://doi.org/10.1074/jbc.M114.596676)
- Heller MJ, Nili M, Homsher E, Tobacman LS (2003) Cardiomyopathic tropomyosin mutations that increase thin filament Ca²⁺ sensitivity and tropomyosin N-domain flexibility. *J Biol Chem* 278:41742–41748. doi:[10.1074/jbc.M303408200](https://doi.org/10.1074/jbc.M303408200)
- Hilario E, da Silva SL, Ramos CH, Bertolini MC (2004) Effects of cardiomyopathic mutations on the biochemical and biophysical properties of the human alpha-tropomyosin. *Eur J Biochem* 271:4132–4140. doi:[10.1111/j.1432-1033.2004.04351.x](https://doi.org/10.1111/j.1432-1033.2004.04351.x)
- Hitchcock-DeGregori SE, Singh A (2010) What makes tropomyosin an actin binding protein? A perspective. *J Struct Biol* 170:319–324. doi:[10.1016/j.jsb.2009.12.013](https://doi.org/10.1016/j.jsb.2009.12.013)
- Hitchcock-DeGregori SE, Song Y, Moraczewska J (2001) Importance of internal regions and the overall length of tropomyosin for actin binding and regulatory function. *Biochemistry* 40:2104–2112
- Holmes KC, Lehman W (2008) Gestalt-binding of tropomyosin to actin filaments. *J Muscle Res Cell Motil* 29:213–219. doi:[10.1007/s10974-008-9157-6](https://doi.org/10.1007/s10974-008-9157-6)
- Hoover WG (1985) Canonical dynamics—equilibrium phase-space distributions. *Phys Rev A* 31:1695–1697
- Humphrey W, Dalke A, Schulten K (1996) VMD: visual molecular dynamics. *J Mol Graph* 14(33–38):27–38
- Im W, Beglov D, Roux B (1998) Continuum solvation model: computation of electrostatic forces from numerical solutions to the Poisson–Boltzmann equation. *Comput Phys Commun* 111:59–75
- Janco M, Kalyva A, Scellini B, Piroddi N, Tesi C, Poggesi C, Geeves MA (2012) alpha-Tropomyosin with a D175N or E180G mutation in only one chain differs from tropomyosin with mutations in both chains. *Biochemistry* 51:9880–9890. doi:[10.1021/bi301323n](https://doi.org/10.1021/bi301323n)
- Jongbloed RJ, Marcelis CL, Doevendans PA, Schmeitz-Mulkens JM, Van Dookum WG, Geraedts JP, Smeets HJ (2003) Variable clinical manifestation of a novel missense mutation in the alpha-tropomyosin (TPM1) gene in familial hypertrophic cardiomyopathy. *J Am Coll Cardiol* 41:981–986
- Kalyva A, Schmidtman A, Geeves MA (2012) In vitro formation and characterization of the skeletal muscle alpha-beta tropomyosin heterodimers. *Biochemistry* 51:6388–6399. doi:[10.1021/bi300340r](https://doi.org/10.1021/bi300340r)
- Karibe A et al (2001) Hypertrophic cardiomyopathy caused by a novel alpha-tropomyosin mutation (V95A) is associated with mild cardiac phenotype, abnormal calcium binding to troponin, abnormal myosin cycling, and poor prognosis. *Circulation* 103:65–71
- Karplus M, McCammon JA (2002) Molecular dynamics simulations of biomolecules. *Nat Struct Biol* 9:646–652. doi:[10.1038/nsb0902-646](https://doi.org/10.1038/nsb0902-646)
- Khaitlina SY (2015) Tropomyosin as a regulator of actin dynamics. *Int Rev Cell Mol Biol* 318:255–291. doi:[10.1016/bs.ircmb.2015.06.002](https://doi.org/10.1016/bs.ircmb.2015.06.002)
- Kremneva E, Boussouf S, Nikolaeva O, Maytum R, Geeves MA, Levitsky DI (2004) Effects of two familial hypertrophic cardiomyopathy mutations in alpha-tropomyosin, Asp175Asn and Glu180Gly, on the thermal unfolding of actin-bound tropomyosin. *Biophys J* 87:3922–3933. doi:[10.1529/biophysj.104.048793](https://doi.org/10.1529/biophysj.104.048793)
- Kwok SC, Hodges RS (2004) Stabilizing and destabilizing clusters in the hydrophobic core of long two-stranded alpha-helical coiled-coils. *J Biol Chem* 279:21576–21588. doi:[10.1074/jbc.M401074200](https://doi.org/10.1074/jbc.M401074200)
- Lakkaraju SK, Hwang W (2009) Modulation of elasticity in functionally distinct domains of the tropomyosin coiled-coil. *Cell Mol Bioeng* 2:57–65. doi:[10.1007/s12195-009-0050-1](https://doi.org/10.1007/s12195-009-0050-1)
- Lehman W, Craig R (2008) Tropomyosin and the steric mechanism of muscle regulation. *Adv Exp Med Biol* 644:95–109
- Lehman W, Li XE, Orzechowski M, Fischer S (2014) The structural dynamics of alpha-tropomyosin on F-actin shape the overlap complex between adjacent tropomyosin molecules. *Arch Biochem Biophys* 552–553:68–73. doi:[10.1016/j.abb.2013.09.011](https://doi.org/10.1016/j.abb.2013.09.011)
- Li MH, Zheng WJ (2011) Probing the structural and energetic basis of kinesin-microtubule binding using computational alanine-scanning mutagenesis. *Biochemistry* 50:8645–8655. doi:[10.1021/Bi2008257](https://doi.org/10.1021/Bi2008257)
- Li M, Zheng W (2012) All-atom structural investigation of kinesin-microtubule complex constrained by high-quality cryo-electron-

- microscopy maps. *Biochemistry* 51:5022–5032. doi:10.1021/bi300362a
- Li XE, Holmes KC, Lehman W, Jung H, Fischer S (2010a) The shape and flexibility of tropomyosin coiled coils: implications for actin filament assembly and regulation. *J Mol Biol* 395:327–339. doi:10.1016/j.jmb.2009.10.060
- Li XE, Lehman W, Fischer S (2010b) The relationship between curvature, flexibility and persistence length in the tropomyosin coiled-coil. *J Struct Biol* 170:313–318. doi:10.1016/j.jsb.2010.01.016
- Li XE, Lehman W, Fischer S, Holmes KC (2010c) Curvature variation along the tropomyosin molecule. *J Struct Biol* 170:307–312. doi:10.1016/j.jsb.2009.12.017
- Li XE, Tobacman LS, Mun JY, Craig R, Fischer S, Lehman W (2011) Tropomyosin position on F-actin revealed by EM reconstruction and computational chemistry. *Biophys J* 100:1005–1013. doi:10.1016/j.bpj.2010.12.3697
- Li XE, Suphamungmee W, Janco M, Geeves MA, Marston SB, Fischer S, Lehman W (2012) The flexibility of two tropomyosin mutants, D175N and E180G, that cause hypertrophic cardiomyopathy. *Biochem Biophys Res Commun* 424:493–496. doi:10.1016/j.bbrc.2012.06.141
- Li XE, Orzechowski M, Lehman W, Fischer S (2014) Structure and flexibility of the tropomyosin overlap junction. *Biochem Biophys Res Commun* 446:304–308. doi:10.1016/j.bbrc.2014.02.097
- Loong CK, Zhou HX, Chase PB (2012a) Familial hypertrophic cardiomyopathy related E180G mutation increases flexibility of human cardiac alpha-tropomyosin. *FEBS Lett* 586:3503–3507. doi:10.1016/j.febslet.2012.08.005
- Loong CK, Zhou HX, Chase PB (2012b) Persistence length of human cardiac alpha-tropomyosin measured by single molecule direct probe microscopy. *PLoS ONE* 7:e39676. doi:10.1371/journal.pone.0039676
- Lorenz M, Poole KJ, Popp D, Rosenbaum G, Holmes KC (1995) An atomic model of the unregulated thin filament obtained by X-ray fiber diffraction on oriented actin-tropomyosin gels. *J Mol Biol* 246:108–119. doi:10.1006/jmbi.1994.0070
- Ly S, Lehrer SS (2012) Long-range effects of familial hypertrophic cardiomyopathy mutations E180G and D175N on the properties of tropomyosin. *Biochemistry* 51:6413–6420. doi:10.1021/bi3006835
- MacKerell AD et al (1998) All-atom empirical potential for molecular modeling and dynamics studies of proteins. *J Phys Chem B* 102:3586–3616
- Mackerell AD Jr, Feig M, Brooks CL 3rd (2004) Extending the treatment of backbone energetics in protein force fields: limitations of gas-phase quantum mechanics in reproducing protein conformational distributions in molecular dynamics simulations. *J Comput Chem* 25:1400–1415. doi:10.1002/jcc.20065
- Marston SB (2011) How do mutations in contractile proteins cause the primary familial cardiomyopathies? *J Cardiovasc Transl Res* 4:245–255. doi:10.1007/s12265-011-9266-2
- Marston S et al (2013) Mutations in repeating structural motifs of tropomyosin cause gain of function in skeletal muscle myopathy patients. *Hum Mol Genet* 22:4978–4987. doi:10.1093/hmg/ddt345
- Marttila M et al (2012) Abnormal actin binding of aberrant beta-tropomyosins is a molecular cause of muscle weakness in TPM2-related nemaline and cap myopathy. *Biochem J* 442:231–239. doi:10.1042/BJ20111030
- Martyna GJ, Hughes A, Tuckerman ME (1999) Molecular dynamics algorithms for path integrals at constant pressure. *J Chem Phys* 110:3275–3290
- Matyushenko AM, Artemova NV, Sluchanko NN, Levitsky DI (2015) Effects of two stabilizing substitutions, D137L and G126R, in the middle part of alpha-tropomyosin on the domain structure of its molecule. *Biophys Chem* 196:77–85. doi:10.1016/j.bpc.2014.10.001
- McKillop DF, Geeves MA (1993) Regulation of the interaction between actin and myosin subfragment 1: evidence for three states of the thin filament. *Biophys J* 65:693–701. doi:10.1016/S0006-3495(93)81110-X
- McLachlan AD, Stewart M, Smillie LB (1975) Sequence repeats in alpha-tropomyosin. *J Mol Biol* 98:281–291
- Michele DE, Coutu P, Metzger JM (2002) Divergent abnormal muscle relaxation by hypertrophic cardiomyopathy and nemaline myopathy mutant tropomyosins. *Physiol Genomics* 9:103–111. doi:10.1152/physiolgenomics.00099.2001
- Mijailovich SM, Kayser-Herold O, Li X, Griffiths H, Geeves MA (2012) Cooperative regulation of myosin-S1 binding to actin filaments by a continuous flexible Tm–Tn chain. *Eur Biophys J EBJ* 41:1015–1032. doi:10.1007/s00249-012-0859-8
- Minakata S, Maeda K, Oda N, Wakabayashi K, Nitanai Y, Maeda Y (2008) Two-crystal structures of tropomyosin C-terminal fragment 176–273: exposure of the hydrophobic core to the solvent destabilizes the tropomyosin molecule. *Biophys J* 95:710–719. doi:10.1529/biophysj.107.126144
- Mirza M et al (2007) The effect of mutations in alpha-tropomyosin (E40K and E54K) that cause familial dilated cardiomyopathy on the regulatory mechanism of cardiac muscle thin filaments. *J Biol Chem* 282:13487–13497. doi:10.1074/jbc.M701071200
- Moore JR, Li X, Nirody J, Fischer S, Lehman W (2011) Structural implications of conserved aspartate residues located in tropomyosin's coiled-coil core. *Bioarchitecture* 1:250–255. doi:10.4161/bioa.18117
- Muthuchamy M et al (1999) Mouse model of a familial hypertrophic cardiomyopathy mutation in alpha-tropomyosin manifests cardiac dysfunction. *Circ Res* 85:47–56
- Nakajima-Taniguchi C, Matsui H, Nagata S, Kishimoto T, Yamauchi-Takahara K (1995) Novel missense mutation in alpha-tropomyosin gene found in Japanese patients with hypertrophic cardiomyopathy. *J Mol Cell Cardiol* 27:2053–2058
- Nina M, Beglov D, Roux B (1997) Atomic radii for continuum electrostatics calculations based on molecular dynamics free energy simulations. *J Phys Chem B* 101:5239–5248
- Olson MA, Reinke LT (2000) Modeling implicit reorganization in continuum descriptions of protein–protein interactions. *Proteins* 38:115–119. doi:10.1002/(SICI)1097-0134(200010)38:1<115:AID-PROT11>3.0.CO;2-P
- Orzechowski M, Fischer S, Moore JR, Lehman W, Farman GP (2014) Energy landscapes reveal the myopathic effects of tropomyosin mutations. *Arch Biochem Biophys* 564:89–99. doi:10.1016/j.abb.2014.09.007
- Phillips GN Jr (1986) Construction of an atomic model for tropomyosin and implications for interactions with actin. *J Mol Biol* 192:128–131
- Phillips GN Jr, Fillers JP, Cohen C (1986) Tropomyosin crystal structure and muscle regulation. *J Mol Biol* 192:111–131
- Phillips JC et al (2005) Scalable molecular dynamics with NAMD. *J Comput Chem* 26:1781–1802. doi:10.1002/jcc.20289
- Pirani A, Xu C, Hatch V, Craig R, Tobacman LS, Lehman W (2005) Single particle analysis of relaxed and activated muscle thin filaments. *J Mol Biol* 346:761–772. doi:10.1016/j.jmb.2004.12.013
- Pirani A et al (2006) An atomic model of the thin filament in the relaxed and Ca²⁺-activated states. *J Mol Biol* 357:707–717. doi:10.1016/j.jmb.2005.12.050
- Poole KJ et al (2006) A comparison of muscle thin filament models obtained from electron microscopy reconstructions and low-angle X-ray fibre diagrams from non-overlap muscle. *J Struct Biol* 155:273–284. doi:10.1016/j.jsb.2006.02.020

- Prabhakar R, Boivin GP, Grupp IL, Hoit B, Arteaga G, Solaro RJ, Wiczorek DF (2001) A familial hypertrophic cardiomyopathy alpha-tropomyosin mutation causes severe cardiac hypertrophy and death in mice. *J Mol Cell Cardiol* 33:1815–1828. doi:10.1006/jmcc.2001.1445
- Redwood C, Robinson P (2013) Alpha-tropomyosin mutations in inherited cardiomyopathies. *J Muscle Res Cell Motil* 34:285–294. doi:10.1007/s10974-013-9358-5
- Roux B (1997) Influence of the membrane potential on the free energy of an intrinsic protein. *Biophys J* 73:2980–2989. doi:10.1016/S0006-3495(97)78327-9
- Rynkiewicz MJ, Schott V, Orzechowski M, Lehman W, Fischer S (2015) Electrostatic interaction map reveals a new binding position for tropomyosin on F-actin. *J Muscle Res Cell Motil*. doi:10.1007/s10974-015-9419-z
- Sharp KA, Honig B (1990a) Calculating total electrostatic energies with the nonlinear Poisson–Boltzmann equation. *J Phys Chem* 94:7684–7692
- Sharp KA, Honig B (1990b) Electrostatic interactions in macromolecules: theory and applications. *Annu Rev Biophys Chem* 19:301–332. doi:10.1146/annurev.bb.19.060190.001505
- Singh A, Hitchcock-DeGregori SE (2006) Dual requirement for flexibility and specificity for binding of the coiled-coil tropomyosin to its target, actin. *Structure* 14:43–50. doi:10.1016/j.str.2005.09.016
- Sousa D, Cammarato A, Jang K, Graceffa P, Tobacman LS, Li XE, Lehman W (2010) Electron microscopy and persistence length analysis of semi-rigid smooth muscle tropomyosin strands. *Biophys J* 99:862–868. doi:10.1016/j.bpj.2010.05.004
- Sousa DR, Stagg SM, Stroupe ME (2013) Cryo-EM structures of the actin: tropomyosin filament reveal the mechanism for the transition from C- to M-state. *J Mol Biol* 425:4544–4555. doi:10.1016/j.jmb.2013.08.020
- Stone JE, Hardy DJ, Ufimtsev IS, Schulten K (2010) GPU-accelerated molecular modeling coming of age. *J Mol Graph Model* 29:116–125. doi:10.1016/j.jmgl.2010.06.010
- Sumida JP, Wu E, Lehrer SS (2008) Conserved Asp-137 imparts flexibility to tropomyosin and affects function. *J Biol Chem* 283:6728–6734. doi:10.1074/jbc.M707485200
- Van Driest SL, Will ML, Atkins DL, Ackerman MJ (2002) A novel TPM1 mutation in a family with hypertrophic cardiomyopathy and sudden cardiac death in childhood. *Am J Cardiol* 90:1123–1127
- Vibert P, Craig R, Lehman W (1997) Steric-model for activation of muscle thin filaments. *J Mol Biol* 266:8–14. doi:10.1006/jmbi.1996.0800
- von der Ecken J, Muller M, Lehman W, Manstein DJ, Penczek PA, Raunser S (2015) Structure of the F-actin–tropomyosin complex. *Nature* 519:114–117. doi:10.1038/nature14033
- Wang F et al (2011) Facilitated cross-bridge interactions with thin filaments by familial hypertrophic cardiomyopathy mutations in alpha-tropomyosin. *J Biomed Biotechnol* 2011:435271. doi:10.1155/2011/435271
- Yamauchi-Takahara K, Nakajima-Taniguchi C, Matsui H, Fujio Y, Kunisada K, Nagata S, Kishimoto T (1996) Clinical implications of hypertrophic cardiomyopathy associated with mutations in the alpha-tropomyosin gene. *Heart* 76:63–65
- Yar S et al (2013) Conserved Asp-137 is important for both structure and regulatory functions of cardiac alpha-tropomyosin (alpha-TM) in a novel transgenic mouse model expressing alpha-TM-D137L. *J Biol Chem* 288:16235–16246. doi:10.1074/jbc.M113.458695
- Yuen M et al (2015) Muscle weakness in TPM3-myopathy is due to reduced Ca²⁺-sensitivity and impaired acto-myosin cross-bridge cycling in slow fibres. *Hum Mol Genet* 24:6278–6292. doi:10.1093/hmg/ddv334
- Zheng X, Diraviyam K, Sept D (2007) Nucleotide effects on the structure and dynamics of actin. *Biophys J* 93:1277–1283. doi:10.1529/biophysj.107.109215
- Zheng W, Barua B, Hitchcock-DeGregori SE (2013) Probing the flexibility of tropomyosin and its binding to filamentous actin using molecular dynamics simulations. *Biophys J* 105:1882–1892. doi:10.1016/j.bpj.2013.09.003